Small molecule inhibition of STOML3 oligomerization reverses pathological mechanical hypersensitivity

Christiane Wetzel[1, ‡], Simone Pifferi[1,†], Cristina Picci[1.3], Caglar Gök[1], Diana Hoffmann[1,4], Kiran K. Bali[5], André Lampe[6], Liudmila Lapatsina[1], Raluca Fleischer[1], Ewan St. John Smith[1,7], Valérie Bégay[1], Mirko Moroni[1], Luc Estebanez[1,4], Johannes Kühnemund[1], Jan Walcher[1], Edgar Specker[6], Martin Neuenschwander[6], Jens Peter von Kries[6], Volker Haucke[6], Rohini Kuner[5], James F.A. Poulet[1,4], Jan Schmoranzer[8], Kate Poole[1,2,*, ‡], Gary R. Lewin[1,4*]

[1]Department of Neuroscience, Max Delbrück Center for Molecular Medicine, Robert-Rössle Straße 10, D-13092 Berlin, Germany,

[2]Department of Physiology and EMBL Australia Node for Single Molecule Science, School of Medical Sciences, UNSW, Sydney, Australia

[3]Department of Biomedical Sciences, Section of Cytomorphology, University of Cagliari, Monserrato (CA), Italy

[4]Neuroscience Research Center and Cluster of Excellence NeuroCure, Charité-Universitätsmedizin, Charitéplatz 1, 10117 Berlin Germany.

[5]Institute of Pharmacology, Heidelberg University, Im Neuenheimer Feld 584, D-69120 Heidelberg, Germany

[6]Leibniz-Institut für Molekulare Pharmakologie (FMP), Robert-Roessle-Str. 10, 13125 Berlin, Germany,

[7]Dept. of Pharmacology, University of Cambridge, Tennis Court Rd., Cambridge, CB2 1PD

[8]Freie Universität Berlin, Robert-Roessle-Straße 10, 13125 Berlin, Germany

† Present address: Neurobiology Group, SISSA, International School for Advanced Studies, Via Bonomea 265, 34136 Trieste, Italy

‡ These authors contributed equally to this work

*Correspondence to: glewin@mdc-berlin.de or k.poole@unsw.edu.au

28 **Summary**

29 The skin is equipped with specialized mechanoreceptors that allow the perception of the

30 slightest brush. Indeed some mechanoreceptors can detect even nanometer-scale movements.

31 Movement is transformed into electrical signals via the gating of mechanically-activated ion

32 channels at sensory endings in the skin. The sensitivity of Piezo mechanically-gated ion

33 channels are controlled by stomatin-like protein-3 (STOML3), which is required for normal

34 mechanoreceptor function. Here we identify small molecule inhibitors of STOML3

35 oligomerization that reversibly reduce the sensitivity of mechanically-gated currents in

36 sensory neurons and silence mechanoreceptors *in vivo*. STOML3 inhibitors in the skin also

37 reversibly attenuate fine touch perception in normal mice. Under pathophysiological

38 conditions following nerve injury or diabetic neuropathy the slightest touch can produce pain,

39 and here STOML3 inhibitors can reverse mechanical hypersensitivity. Thus, small molecules

40 applied locally to the skin can be used to modulate touch and may represent peripherally

41 available drugs to treat tactile-driven pain following neuropathy.

42

43

44

45

46

47

48

49

50

51

52

53

54

55

56

Introduction

All skin sensation starts with the transformation of a physical stimulus into an electrical signal called a receptor potential. The receptor potential is encoded as action potentials (AP), which convey information to the brain to initiate perception[1]. Currently pharmacological agents that modulate the first step in the transformation of light touch stimuli into an electrical signal, a process called sensory mechanotransduction, are not available. The mechanosensitive ion channel Piezo2 and its modulator STOML3[2] have both been shown to be necessary for mechanoreceptors to transduce light touch[3–6]. Paradoxically, under pathophysiological conditions, intense pain can also be triggered by light touch[7,8], for example after traumatic nerve injury[9]. Nerve injury induced touch-evoked pain was found to be largely absent in $Stoml3^{-/-}$ mutant mice[6]. STOML3 is an endogenous regulator of the sensitivity of mechanosensitive ion channels like Piezo in sensory neurons and STOML3 self-association appears to be necessary for this function[10,11]. Interestingly, Piezo2 has an essential role in human proprioception and touch sensation[12,13]. Therefore we set out to discover and test whether small molecules that can disrupt STOML3 self-association can be used to modulate touch under normal and pathophysiological conditions.

Identification of small molecule STOML3 inhibitors

In mammals STOML3 belongs to a family of five structurally conserved membrane proteins, including Stomatin, STOML1, STOML2, and Podocin[10,14–18], all of which self-associate via their stomatin-domain (Supplementary Fig. S1a)[10]. Self-association of stomatin-domain proteins can be monitored in HEK293 cells using Bimolecular Fluorescence Complementation (BiFC) whereby N- and C-terminal halves of the YFP molecule are tagged to the prey and bait protein STOML3[2,19] (Fig. 1a). Irreversible association of the YFP fragments produces fluorescence that increases linearly over time (Fig. 1 b). Mutations in one STOML3 pair that disrupt oligomerization (V190P or LR89,90EE) significantly reduce the

82   rate of signal development (Fig.   1b)[2,10]. We used this cellular assay in a high throughput

83   format to screen for small molecules that significantly inhibit the BiFC signal, a measure of

84   STOML3 self-association. In a primary screen of about 35000 small molecules (each at 20

85   µM), obtained from the central compound collection of the Leibniz Institute for Molecular

86   Pharmacology screening unit (www.chembionet.info), 21 molecules were found to

87   reproducibly decrease STOML3 self-association based on the slope of YFP signal

88   development. Of these 21 molecules 19 did not pass stringent control tests (see Materials and

89   Methods). The two remaining inhibitory compounds were designated Oligomerization

90   Blocker 1 and 2, (OB-1 and OB-2) (Fig. 1d,e). In further BiFC assays, the STOML3

91   oligomerization blocker, OB-1 was an effective inhibitor of the self-association of Stomatin,

92   STOML1, STOML2, but not Podocin (Supplementary Fig. 1a). Lower OB-1 concentrations

93   (2 µM) also inhibited the BiFC signal (Supplementary Fig. 1b). The OB-1 molecule was also

94   re-synthesized in house and exhibited the same activity in the BiFC assay as the

95   commercially available sample. The human STOML3 peptide sequence is 92% identical to

96   that of the mouse and 100% identical in the core stomatin-domain and human STOML3 also

97   showed self-association (Fig. 1f). More importantly for potential future clinical development

98   self-association of the human STOML3 protein was also inhibited by OB-1 (Fig 1f).

99   **STOML3 oligomerization dictates domain size in the plasma membrane**

100   We next asked if OB-1 and OB-2 modulation of STOML3 oligomerization state influences

101   clustering of the protein in the plasma membrane. We used super-resolution dSTORM

102   microscopy[20–22] to visualize FLAG–tagged STOML3 at the plasma membrane of transfected

103   N2a cells. Using dSTORM we could show that STOML3 was present in microdomains at the

104   plasma membrane (Fig. 1g). The size of the STOML3 clusters was variable (full width at half

105   maximum, FWHM = 24.6 ± 2.8 nm, mean ± sem, Fig. 1h.) but these domains may contain

106   more   than   one   STOML3   dimer[10].   Introduction   of   the   V190P   mutation   disrupts

107 oligomerization of STOML3 and abolishes its ability to modulate the mechanosensitivity of

108 Piezo1 channels[2]. This STOML3 variant exhibited significantly smaller clusters in the plasma

109 membrane (Fig. 1g,h), demonstrating that by disrupting STOML3 oligomerization we can

110 manipulate and measure nanoscale changes in STOML3 cluster size. Pre-incubation of N2a

111 cells expressing STOML3-FLAG with OB-1 or OB-2 for three hours led to significantly

112 reduced STOML3-FLAG cluster sizes compared to vehicle treated cells (Fig. 1g,h). The

113 effects of OB-1 did not produce changes in *Stoml3* mRNA levels in these cells

114 (Supplementary Fig. 2a). Thus we obtained independent support for the notion that OB-1 and

115 OB-2 reduce STOML3 oligomerization state, an important consequence of which is a

116 reduced STOML3 cluster size at the plasma membrane.

117 **STOML3 inhibitors modulate mechanotransduction currents**

118 Endogenously expressed STOML3 in N2a cells is required to maintain Piezo channel

119 sensitivity to membrane deflection[2]. By precisely deflecting defined areas of the membrane-

120 substrate interface using a pillar array we could activate Piezo1 currents in N2a cells with

121 displacements ranging from 100 - 1000 nm (Fig. 2a,b). Both OB-1 and OB-2 reduced the

122 sensitivity of mechanosensitive currents to pillar deflection (Fig. 2b). Pre-incubation of cells

123 with OB-1 for periods of between 1 and 3 h reduced Piezo1 current amplitudes, but the effect

124 was only maximal after 3 h (Supplementary Fig. 2b). Recording mechanically-activated

125 currents in the presence of different concentrations of OB-1 revealed a steep concentration

126 dependence with a calculated IC_{50} of 10 nM, Hill coefficient 0.6 (Fig. 2c).

127 Next we evaluated the effects of OB-1 and OB-2 on mechanosensitive currents in acutely

128 cultured mouse sensory neurons. Neurons were classified on the basis of their AP

129 configuration as mechanoreceptors or nociceptors[2,23]. We found that mechanically gated

130 currents in mechanoreceptors start to activate with membrane deflections of < 50 nm[2], but

131 this sensitivity was substantially reduced after exposure to OB-1 or OB-2 (Fig. 2 d,e). Thus

132   significant mechanically gated currents were only observed in OB-1 or OB-2 treated cells

133   with deflections that exceeded 100 nm. The threshold for activation of mechanosensitive

134   currents in nociceptive sensory neurons is normally higher than that of mechanoreceptors[2] a

135   finding reproduced here (Fig. 2e,f). However, we also observed that OB-1 or OB-2 treatment

136   produced a significant reduction in the amplitude of mechanically gated currents in

137   nociceptors with stimulus magnitudes between 100 and 500 nm (Fig. 2f). In addition the

138   latency for mechanically gated currents as well as the activation time constant for current

139   activation τ_1 was significantly slowed in nociceptors after treatment with OB-2

140   (Supplementary Fig. 2 c,d). The exposure of N2a cells or sensory neurons to OB-1 for 3h did

141   not lead to any changes in the level of *Stoml3* transcripts (Supplementary Fig. 2a), suggesting

142   that our molecules change gene expression, or transcript stability. Cell soma indentation can

143   also be used to evoke so called Rapidly-adapting currents (RA-currents, inactivation constant

144     $\tau_2 < 5$ ms) in mechanoreceptor sensory neurons[23,24] and after exposure to OB-1 ~ 60% of the

145   neurons (12/21 neurons) displayed no mechanosensitive current compared to control or

146   vehicle treated neurons (21%, 8/38 neurons), this effect was statistically significant (Fisher's

147   exact test p < 0.01 Supplementary Fig. 3a-e). Neither of the two compounds tested had any

148   discernable effects on voltage-gated currents or membrane excitability as evidenced by the

149   fact that APs were of normal amplitude and shape after treatment (Fig. 2h,i). For example,

150   cultured sensory neurons treated for at least 3 h with 20 μM OB-1 displayed no alteration in a

151   number of parameters indicative of electrical excitability (Fig 2g-i, Supplementary Table 1).

152   In summary, using two independent assays we found that OB-1 is a powerful inhibitor of

153   native mechanosensitive currents. Stomatin-domain proteins can also negatively regulate

154   members of the <u>a</u>cid <u>s</u>ensing <u>i</u>on <u>c</u>hannel family (ASICs) in a subunit-specific manner

155   [6,10,25,26]. However, OB-1 had no detectable effect on the negative modulation of ASIC3

156   mediated currents by mouse Stomatin (Supplementary Fig. 4).

A STOML3 inhibitor can silence touch receptors

Many cutaneous mechanoreceptors in *Stoml3*^{-/-} mice innervate the skin, but cannot be activated by mechanical stimulation[5,6]. We made subcutaneous injections of the OB-1 compound (250 - 500 pmol per paw) into the mouse hairy skin innervated by the saphenous nerve and recorded from sensory afferents 3 h later using an *ex vivo* skin - nerve preparation[5,27]. In wild type mice the vast majority of myelinated and unmyelinated fibers are mechanosensitive[4–6], demonstrated by tracing the spike evoked by local electrical stimulation of nerve branches and then searching for the nearby mechanosensitive receptive field (Fig. 3a). In contrast, in skin pre-treated with OB-1 over 39% of Aβ-fibers (19/44) lacked a mechanosensitive receptive field, and this was significantly different from vehicle-injected controls where less than 7% (5/69 fibers) were found to be insensitive to mechanical stimuli, $p < 0.001$ Fischer's exact test (Fig. 3a, Supplementary Table 2). An almost identical proportion of OB-1 treated Aβ-fibers were insensitive to mechanical stimuli in female mice as in male mice (Fig. 3a). Amongst the Aδ-fibers we also observed an increase in the proportion of fibers for which no mechanosensitive receptive field could be found (21%, 8/38 fibers compared to 6%, 1/19 fibers in controls, but this was not significantly different; Fischer's exact test, $p > 0.24$). There was also no change in the proportion of C-fibers that lack a mechanosensitive receptive field (Fig. 3a). We next examined the physiological properties of the remaining mechanosensitive afferents in OB-1 treated skin. However, the proportion of mechanoreceptor types found, as well as the mechanosensitivity of the remaining Aβ-fiber mechanoreceptors (Rapidly and Slowly adapting mechanoreceptors, RAMs and SAMs) was unchanged compared to controls (Supplementary Fig. 5a-e). The mechanoreceptor silencing effect of local OB-1 treatment was completely reversible as recordings from afferents 24 h after treatment revealed no significant loss of mechanosensitivity, also compared to vehicle treated skin (Fig. 3a). Thus, a STOML3

182   oligomerization inhibitor can specifically and reversibly silence touch receptor activity

183   without changing axonal excitability.

184   Although, we found no evidence that C-fiber nociceptors are silenced by OB-1 treatment

185   (Fig. 3a) we did note a statistically significant effect of local OB-1 treatment on the

186   mechanosensitivity of C-fiber afferents that respond to both thermal and mechanical stimuli

187   (C-mechanoheat fibers, C-MH, Two-way ANOVA, $p < 0.05$) (Fig. 3b). C-mechanoheat

188   fibers also displayed significantly elevated mechanical thresholds for activation that were on

189   average almost twice that of control fibers (196.5 ± 35.6 mN, mean ± sem in OB-1 treated

190   skin *vs* 106.9 ± 17.4 mN, mean ± sem in vehicle treated skin, Mann-Whitney *U* test, $p < 0.05$)

191   as measured using a force measurement system attached to the stimulus probe (Fig. 3c). The

192   firing rates of C-mechanonociceptors (C-Ms) that lack heat sensitivity, to suprathreshold

193   mechanical stimuli were not significantly attenuated in OB-1 treated skin (Fig. 3d,e).

194   **Touch perception is attenuated by local OB-1 treatment**

195   We used a tactile perception task in head-restrained mice to assess the effects of OB-1 on

196   touch sensation. Water-restricted mice were trained to press a sensor with their forepaw

197   within 500 ms after the onset of a 30 ms cosine mechanical stimulus applied to the same paw.

198   Correct responses were rewarded with water. Mice learned this task to a high degree of

199   reliability after a 7-10 day training period (Fig. 4a). Different stimulus amplitudes were then

200   used to determine a psychometric curve for each mouse (Fig. 4a,b). We next injected the drug

201   vehicle solution into the forepaw and obtained a new psychometric curve for each mouse 3 -

202   5 h later. On the next day, the forepaw was injected with the OB-1 compound (11 nmol per

203   paw) followed by behavioral testing. At least 24 h after the OB-1 testing day, the recovery

204   behavior was tested without any prior injection. Following OB-1 treatment the psychometric

205   curve was shifted to the right for stimulus strengths between 125-275 µm indicating less

206   reliable stimulus detection (Wilcoxon Signed Rank Test, vehicle *vs* OB-1, $p = 0.026$; OB-1 *vs*

207 recovery, p = 0.0043) (Fig. 4 b,c). Vehicle treatment produced no significant change in the

208 psychometric curve (Wilcoxon Signed Rank Test, control *vs* vehicle p = 0.30). The detection

209 rates of threshold stimuli returned to pre-treatment levels 1-4 d after treatment (Wilcoxon

210 Signed Rank Test, vehicle *vs* recovery, p = 0.12). These data indicate that silencing of a

211 subset of mechanoreceptors via STOML3 inhibition is sufficient to reduce the reliability of

212 near threshold touch perception in mice.

213 **Peripheral STOML3 blockade reverses tactile allodynia**

214 Neuropathic pain is a debilitating condition in which intense pain can be initiated by merely

215 brushing the skin, activating low-threshold mechanoreceptors[7–9,28,29]. We used the chronic

216 constriction injury model (CCI), which involves direct damage to sciatic nerve axons

217 (Supplementary Fig. 6a-f) that innervate the hypersensitive plantar hindpaw skin. Baseline

218 paw withdrawal thresholds in wild type and *Stoml3*^{-/-} mice did not differ, as measured with

219 von Frey hairs using an adapted up-down method[30] (Fig. 5a). However, after induction of a

220 unilateral CCI[9], paw withdrawal thresholds dropped profoundly in wild type mice but were

221 only moderately reduced in *Stoml3*^{-/-} mice, Two-way ANOVA, p < 0.001 (Fig. 5a). Thermal

222 hyperalgesia also accompanies neuropathic injury[7,9,31], a phenomenon that we also observed.

223 However, the heat hyperalgesia observed in *Stoml3*^{-/-} mice was identical to that in wild type

224 controls (Fig. 5b).

225 We next asked whether local application of OB-1 can ameliorate tactile-evoked pain behavior

226 in neuropathic models. We found no change in paw withdrawal thresholds to mechanical

227 stimuli in the paws of naïve mice treated with an intraplantar dose of OB-1 (250 - 500 pmol

228 per paw) (Fig. 5c). However, when we applied an intraplantar dose of OB-1 to the paws of

229 wild type mice with established neuropathic pain (CCI model 6 - 21 days after induction) we

230 observed a complete reversal of the tactile-evoked pain or allodynia, 0.15 ± 0.06 g (CCI) *vs*

231 0.7125 ± 0.12 g (OB-1 treated p = 0.0028; paired t-test (Fig. 5d). The effects of OB1 were

232   also indistinguishable on female and male mice with CCI (Fig 5d)[32]. We also applied OB-1 to

233   the contralateral paw at the same concentration that was effective at reversing allodynia

234   present in the paw ipsilateral to the injury, but observed no reversal of established

235   hypersensitivity (Fig 5e). These results suggest that the actions of OB-1 in reversing

236   hypersensitivity are due to inhibition of sensory neuron mechanotransduction in the skin and

237   not to systemic or central actions. The reversal of tactile allodynia observed with local OB-1

238   treatment was indistinguishable from that found with systemic gabapentin treatment (Fig. 5f),

239   a standard, centrally acting drug, in clinical use for the treatment of neuropathic pain [33].

240   Using a series of OB-1 concentrations we could determine a half-maximal effective dose

241   (ED_{50}) of 4.42 µM (or approximately 20 pmol per paw) (Fig. 5g). The effects of a single OB-

242   1 dose became maximal 3 h after the injections and wore off slowly over the next 12 h so that

243   the effect was absent after 24 h (Fig. 5h). To test the idea that OB-1 reverses mechanical

244   hypersensitivity primarily by inhibiting STOML3 oligomerization we tested the effects of

245   local OB-1 on the mechanical sensitivity of $Stoml3^{-/-}$ mice with CCI. Mechanical

246   hypersensitivity following CCI is much less prominent in $Stoml3^{-/-}$ mice (Fig. 5a,i) but we

247   observed no change in paw withdrawal threshold after treatment of neuropathic paws of

248    $Stoml3^{-/-}$ mice with OB-1 (Fig. 5i). Off-target effects are an issue for any biologically active

249   small molecule. We therefore tested the effects of 20µM OB-1 in a commercially available *in*

250   *vitro* pharmacology panel (www.cerep.fr) consisting of 79 receptors and ion channels (see

251   Supplementary Dataset 1). Significant inhibition of specific ligand binding to the selected

252   receptors was seen in a few cases (6/79), but there is at present no data implicating any of

253   these receptors in peripheral nociception. The agreement between the *in vitro* and *in vivo*

254   effects of STOML3 inhibition and the results of genetic ablation of the *Stoml3* in the mouse

255   suggest that OB-1 exerts its biological effects primarily on STOML3. The remarkable

256   protection from touch-evoked pain in animals lacking STOML3 led us to hypothesize that the

257 nerve injury may itself lead to a change in the levels of *Stoml3* mRNA expression in the

258 DRG. Up-regulation of STOML3 could in turn exacerbate touch-evoked pain by enhancing

259 the sensitivity of mechanotransduction in injured sensory afferents. Using real-time

260 quantitative PCR we measured a doubling in *Stoml3* mRNA expression levels in the lumbar

261 DRGs that project axons to the ligation site compared to the control uninjured side ($p<0.01$;

262 Mann-Whitney U-test) (Fig. 5j).

263 The CCI model involves direct damage to the axons that innervate the hypersensitive skin, in

264 this case the plantar hindpaw[34]. Neuropathic touch hypersensitivity is also induced in the

265 same skin area by cutting adjacent nerves to the tibial nerve that innervates the plantar foot

266 [35,36]. Spared tibial nerve injury (SNI) mice develop a long lasting hypersensitivity of similar

267 magnitude to that observed following CCI (Supplementary Fig. 7a). Administration of OB-1

268 to the plantar skin in the SNI model produced no reversal of allodynia (Supplementary Figure

269 7b). We removed the lumbar DRGs from these animals and found no change in the levels of

270 *Stoml3* mRNA between the injured and uninjured side in this model (Supplementary Fig.7c).

271 This finding suggests that the effects of OB-1 in alleviating mechanical hypersensitivity may

272 in part depend on whether STOML3 levels are up-regulated.

273 Mechanical hyperalgesia is also a prominent feature in inflammatory pain, which is largely

274 dependent on increased nerve growth factor (NGF) levels[37]. Systemic dosing with NGF (1

275 mg/kg) is sufficient to provoke long-lasting mechanical and heat hyperalgesia[37,38], which

276 were both unchanged in NGF-injected *Stoml3*^{-/-} mice (Supplementary Fig. 7d,e).

277 Additionally, mechanical hypersensitivity after NGF was also not reversed by local

278 intraplantar OB-1 (Supplementary Fig. 7f,g). This data is consistent with the prevailing view

279 that NGF-dependent cutaneous mechanical hyperalgesia is primarily driven by central

280 sensitization[37,39].

281 **Regulation of *Stoml3* mRNA and protein after injury**

282   The levels of *Stoml3* mRNA are very low in the DRG and we have never found an antibody

283   that is sensitive or specific enough to detect endogenous STOML3. We therefore generated

284   two new knock-in mouse models to monitor in the first case *Stoml3* gene expression and in

285   the second case STOML3 protein. We created a knockin allele in which a β-galactosidase

286   cassette with a nuclear localization signal (NLS) was fused in frame with the start codon of

287   the *Stoml3* gene (*Stoml3*[lacZ] mice) (Supplementary Fig. 8 a-c). This reporter allele allowed us

288   to visualize subsets of sensory neurons that express *Stoml3* (Fig. 6a). We observed lacZ

289   staining in around half of sensory neurons with cell bodies > 20 μm in diameter, a population

290   known to consist of mechanoreceptors (Fig. 6a). The number of lacZ-positive neurons more

291   than doubled in the L6-L4 ganglia after a unilateral CCI challenge and the cells were

292   predominantly > 20 μm in diameter, Fisher's exact test, $p < 0.0001$ (Fig. 6b). This data is

293   consistent with the idea that chronic nerve constriction leads to an increase in the number of

294   large and medium sized sensory neurons that express higher levels of *Stoml3*. Consistent with

295   our observation that *Stoml3* mRNA levels are very low in the DRG, the LacZ-positive cells

296   were difficult to visualize when screening for β-galactosidase activity and antibodies directed

297   against the β-galactosidase protein did not give staining. It was therefore difficult to obtain a

298   neurochemical profile of *Stoml3* expressing sensory neurons.

299   In the second knock-in mouse we introduced nucleotides encoding the StrepII tag[40] 3' to the

300   start codon (Fig 6c, Supplementary Fig. 8d-f). The genomic fusion was successful as we

301   could amplify *Stoml3* mRNA transcripts containing the nucleotide sequence encoding an N-

302   terminally StrepII-tagged *Stoml3*. We carried out Western blotting for the StrepII-tagged

303   protein in *Stoml3*[StrepII] CCI mice and extracted protein from sciatic nerve at day 2, day 6 and

304   day 13 post-injury. We could detect a specific band (absent in *Stoml3*^{-/-} nerve) of the

305   appropriate molecular weight in protein extracts from the sciatic nerve, but only after using a

306   strong denaturing buffer containing 8M urea (Fig 6d). We could sometimes detect the

307　StrepII-STOML3 band from extracts made from DRG but this was much weaker and less

308　reliable (data not shown). Notably, we found more intense -STOML3-StrepII positive bands

309　on the injured side at day 2, day 6 and to a lesser extent at day 13 compared to the non-

310　injured contralateral nerve (Fig. 6d). The fact that the neuronal marker PGP9.5 band,

311　dramatically decreased in intensity on the injured side several days after injury, probably

312　reflects axon loss and atrophy, despite this STOML3 levels were increased. These results

313　suggest that endogenous STOML3 is transported preferentially to the peripheral endings of

314　sensory neurons[41] to modulate mechanotransduction and that there is more STOML3

315　transported to sensory endings after traumatic nerve injury.

316　**STOML3 and painful diabetic neuropathy**

317　Neuropathy is a prominent symptom of diabetes, and is often characterized by pain initiated

318　by normally innocuous tactile stimulation in up to 20% of all patients[42]. We next asked

319　whether OB-1 shows efficacy in a mouse model of painful diabetic neuropathy. We used the

320　streptozotocin model (STZ) to induce mechanical hypersensitivity in mice with diabetes[43].

321　Between 6-7 weeks after STZ treatment, mice assigned to the drug and vehicle group began

322　to display hypersensitivity to mechanical stimuli as reflected in increased frequency of paw

323　withdrawal to von Frey filaments below 0.5 g (Fig. 7 a-d). Local treatment of the hindpaw

324　glabrous skin with OB-1 (250 pmol per paw) substantially reversed the mechanical

325　hypersensitivity 4 h after treatment whereas vehicle treatment was without effect (Fig 7a-d),

326　PWT = 0.93 ± 0.13 g (OB-1 treated) *vs* 0.32 ± 0.06 (STZ), paired t-test, p = 0.0013 (Fig. 7b)

327　or PWT = 0.63± 0.13 g (vehicle treated) *vs* 0.51± 0.01 (STZ), paired t-test, p = 0.31 (Fig.

328　7d). The mechanical hypersensitivity returned to pre-drug treatment levels 24 h after a single

329　treatment, as assessed by the mean 60% withdrawal threshold (Fig. 7a,b).

330

331

Discussion

Mammalian touch sensation is at last beginning to be unraveled at the molecular level[44,45]. Mechanosensitive ion channels, like Piezo1 and Piezo2, may prove difficult targets to exploit for pharmacological intervention[46]. For example, the early embryonic or post-natal lethality associated with *Piezo1* or *Piezo2* gene deletion[47,48] and Piezo2's role in proprioception[12,13,49] could prove problematic for the development of Piezo antagonists for therapeutic purposes. Here we describe an intersectional approach to modulate sensory mechanotransduction as our compounds should only be effective in cells in which both STOML3 and Piezo channels are present. This approach has the advantage that essential functions of Piezo proteins will not be directly affected by our small molecules yet we can gain selective and powerful inhibition of sensory mechanotransduction, especially under some pathophysiological conditions. We show that OB-1 has a powerful silencing effect on around 40% of mechanoreceptors and conclude that the transformation of the mechanical stimulus into receptor potential is severely impaired in these cells. Mechanosensitive currents were also inhibited by OB-1 in some nociceptors in our in vitro studies (Fig. 2f) and consistent with this mechanical thresholds were significantly elevated in many cutaneous C-fibers measured using the *ex vivo* skin-nerve preparation (Fig. 3). We propose that STOML3 inhibition silences mechanoreceptors primarily by reducing the displacement sensitivity of Piezo2 ion channels in mechanoreceptors. Mechanically gated currents in nociceptors may not be dependent on Piezo2[4], but deep sequencing studies have detected Piezo1 transcripts in many single mouse sensory neurons[50] and Piezo1 channels are also strongly modulated by STOML3[2]. Skin application of our STOML3 inhibitor OB-1 shows remarkable efficacy in reducing touch-evoked pain behavior in two mouse models of neuropathic pain, but not in an SNI model. There is direct damage to the axons that innervate the sensitized skin in the CCI model that is associated with increased *Stoml3* expression as well as increased STOML3 protein transport

357 to the periphery (Fig. 6). Thus, we speculate that the remarkable efficacy of OB-1 in some

358 pain models, including painful diabetic neuropathy is directly linked to changes in STOML3

359 availability at sensory endings during disease progression. Stoml3 mRNA transcript

360 expression has been detected in human tibial nerve and skin (http://gtexportal.org) and so it

361 may be possible to detect changes in STOML3 in pathologies associated with neuropathic

362 pain. In summary, we provide mechanistic validation of a novel pharmacological strategy to

363 modulate sensory mechanotransduction to treat sensory disorders including pain.

364 **Accession Codes**

365 N/A

366 **Data Availability Statement**

367 All materials and datasets are available on request

368 **Acknowledgements**

385 **Author Contributions**

386 KP designed and carried out the screen, and characterized small molecules with dSTORM

387 and patch clamp electrophysiology. CW performed ex vivo skin electrophysiology and

experiments in mice and behavioral experiments. SP screened OB-1 for effects on mechanosensitive currents in DRGs. CP performed behavioral and real time PCR experiments and performed histochemical analysis of the *Stoml3^{lacz}* mice. CG determined IC50s using the pili method. DH performed touch perception assays with LE who established the methodology. KKB established the diabetic neuropathay model and performed behavioral experiments. AL performed and analyzed *d*STORM experiments with LL, VB, KP, CP and JW generated and characterized the *Stoml3^{lacz}* and *Stoml^{StrepII}* mice. LL and RF performed molecular cloning experiments. Est.JS performed ASIC experiments. MM performed additional electrophysiological experiments. JK analysed transmission electron microscopy data. ES synthesized molecules and managed compound libraries. MN performed statistical analyses of high throughput screening data and helped in design and execution of the screen. JPvK supervised screening experiments. JFAP established touch perception assays and supervised the acquisition and analysis of the data. VH and JS directed and supervised imaging experiments. KP, CW and GRL wrote the paper. KP, CW and GRL conceived and directed the project.

Competing Financial Interests Statement

G.R.L., K.P.,C.W., E.S., L.L. are named as inventors on a patent application related to data in this paper.

References

1. Bensmaia, S. J. Tactile intensity and population codes. *Behav. Brain Res.* **190,** 165–173 (2008).

2. Poole, K., Herget, R., Lapatsina, L., Ngo, H.-D. & Lewin, G. R. Tuning Piezo ion channels to detect molecular-scale movements relevant for fine touch. *Nat. Commun.* **5,** 3520 (2014).

3. Woo, S.-H. *et al.* Piezo2 is required for Merkel-cell mechanotransduction. *Nature* (2014). doi:10.1038/nature13251

4. Ranade, S. S. *et al.* Piezo2 is the major transducer of mechanical forces for touch sensation in mice. *Nature* **516,** 121–125 (2014).

5. Moshourab, R. A., Wetzel, C., Martinez-Salgado, C. & Lewin, G. R. Stomatin-domain protein interactions with acid-sensing ion channels modulate nociceptor mechanosensitivity. *J. Physiol.* **591,** 5555–5574 (2013).

6. Wetzel, C. *et al.* A stomatin-domain protein essential for touch sensation in the mouse. *Nature* **445,** 206–209 (2007).

421   7.   Costigan, M., Scholz, J. & Woolf, C. J. Neuropathic pain: a maladaptive response of

422   the nervous system to damage. *Annu. Rev. Neurosci.* **32,** 1–32 (2009).

423   8.   von Hehn, C. A., Baron, R. & Woolf, C. J. Deconstructing the Neuropathic Pain

424   Phenotype to Reveal Neural Mechanisms. *Neuron* **73,** 638–652 (2012).

425   9.   Tal, M. & Bennett, G. J. Extra-territorial pain in rats with a peripheral

426   mononeuropathy: mechano-hyperalgesia and mechano-allodynia in the territory of an

427   uninjured nerve. *Pain* **57,** 375–382 (1994).

428   10.   Brand, J. *et al.* A stomatin dimer modulates the activity of acid-sensing ion channels.

429   *EMBO J.* **31,** 3635–3646 (2012).

430   11.   Poole, K. *et al.* Tuning Piezo ion channels to detect molecular-scale movements

431   relevant for fine touch. *Nat. Commun.* **5,** 3520 (2014).

432   12.   Chesler, A. T. *et al.* The Role of *PIEZO2* in Human Mechanosensation. *N. Engl. J.*

433   *Med.* **375,** 1355–1364 (2016).

434   13.   Mahmud, A. A. *et al.* Loss of the proprioception and touch sensation channel PIEZO2

435   in siblings with a progressive form of contractures. *Clin. Genet.* (2016).

436   doi:10.1111/cge.12850

437   14.   Wang, Y. & Morrow, J. S. Identification and characterization of human SLP-2, a novel

438   homologue of stomatin (band 7.2b) present in erythrocytes and other tissues. *J. Biol.*

439   *Chem.* **275,** 8062–8071 (2000).

440   15.   Boute, N. *et al.* NPHS2, encoding the glomerular protein podocin, is mutated in

441   autosomal recessive steroid-resistant nephrotic syndrome. *Nat. Genet.* **24,** 349–354

442   (2000).

443   16.   Mairhofer, M., Steiner, M., Salzer, U. & Prohaska, R. Stomatin-like protein-1 interacts

444   with stomatin and is targeted to late endosomes. *J. Biol. Chem.* **284,** 29218–29229

445   (2009).

446   17.   Da Cruz, S. *et al.* SLP-2 interacts with prohibitins in the mitochondrial inner

447   membrane and contributes to their stability. *Biochim. Biophys. Acta* **1783,** 904–911

448   (2008).

449   18.   Lapatsina, L., Brand, J., Poole, K., Daumke, O. & Lewin, G. R. Stomatin-domain

450   proteins. *Eur. J. Cell Biol.* **91,** 240–245 (2012).

451   19.   Hu, C.-D., Chinenov, Y. & Kerppola, T. K. Visualization of interactions among bZIP

452   and Rel family proteins in living cells using bimolecular fluorescence

453   complementation. *Mol. Cell* **9,** 789–798 (2002).

454   20.   Heilemann, M. *et al.* Subdiffraction-resolution fluorescence imaging with conventional

455   fluorescent probes. *Angew. Chem. Int. Ed. Engl.* **47,** 6172–6176 (2008).

456   21.   Lampe, A., Haucke, V., Sigrist, S. J., Heilemann, M. & Schmoranzer, J. Multi-colour

457   direct STORM with red emitting carbocyanines. *Biol. Cell* **104,** 229–237 (2012).

458   22.   Wolter, S. *et al.* rapidSTORM: accurate, fast open-source software for localization

459   microscopy. *Nat. Methods* **9,** 1040–1041 (2012).

460   23.   Hu, J. & Lewin, G. R. Mechanosensitive currents in the neurites of cultured mouse

461   sensory neurones. *J. Physiol.* **577,** 815–828 (2006).

462   24.   McCarter, G. C., Reichling, D. B. & Levine, J. D. Mechanical transduction by rat

463   dorsal root ganglion neurons in vitro. *Neurosci. Lett.* **273,** 179–182 (1999).

464   25.   Price, M. P., Thompson, R. J., Eshcol, J. O., Wemmie, J. A. & Benson, C. J. Stomatin

465   modulates gating of acid-sensing ion channels. *J. Biol. Chem.* **279,** 53886–53891

466   (2004).

467   26.   Kozlenkov, A., Lapatsina, L., Lewin, G. R. & Smith, E. S. J. Subunit-specific

468   inhibition of acid sensing ion channels by stomatin-like protein 1. *J. Physiol.* **592,**

469   557–569 (2014).

470   27.   Milenkovic, N., Wetzel, C., Moshourab, R. & Lewin, G. R. Speed and temperature

471   dependences of mechanotransduction in afferent fibers recorded from the mouse

472   saphenous nerve. *J. Neurophysiol.* **100,** 2771–2783 (2008).

473   28.   Lewin, G. R. & Moshourab, R. Mechanosensation and pain. *J. Neurobiol.* **61,** 30–44

474   (2004).

475   29.   Beggs, S., Trang, T. & Salter, M. W. P2X4R+ microglia drive neuropathic pain. *Nat.*

476   *Neurosci.* **15,** 1068–1073 (2012).

477   30.   Chaplan, S. R., Bach, F. W., Pogrel, J. W., Chung, J. M. & Yaksh, T. L. Quantitative

478   assessment of tactile allodynia in the rat paw. *J. Neurosci. Methods* **53,** 55–63 (1994).

479   31.   Baron, R. Neuropathic pain: a clinical perspective. *Handb. Exp. Pharmacol.* 3–30

480   (2009). doi:10.1007/978-3-540-79090-7_1

481   32.   Sorge, R. E. *et al.* Different immune cells mediate mechanical pain hypersensitivity in

482   male and female mice. *Nat. Neurosci.* **18,** 1081–1083 (2015).

483   33.   Dworkin, R. H. *et al.* Recommendations for the pharmacological management of

484   neuropathic pain: an overview and literature update. *Mayo Clin. Proc.* **85,** S3-14

485   (2010).

486   34.   Basbaum, A. I., Gautron, M., Jazat, F., Mayes, M. & Guilbaud, G. The spectrum of

487   fiber loss in a model of neuropathic pain in the rat: an electron microscopic study. *Pain*

488   **47,** 359–67 (1991).

489   35.   Decosterd, I. & Woolf, C. J. Spared nerve injury: an animal model of persistent
490   peripheral neuropathic pain. *Pain* **87,** 149–158 (2000).

491   36.   Shields, S. D., Eckert, W. A. & Basbaum, A. I. Spared nerve injury model of
492   neuropathic pain in the mouse: a behavioral and anatomic analysis. *J. Pain Off. J. Am.*
493   *Pain Soc.* **4,** 465–470 (2003).

494   37.   Lewin, G. R., Lechner, S. G. & Smith, E. S. J. Nerve growth factor and nociception:
495   from experimental embryology to new analgesic therapy. *Handb. Exp. Pharmacol.*
496   **220,** 251–282 (2014).

497   38.   Lewin, G. R. *et al.* Nerve growth factor-induced hyperalgesia in the neonatal and adult
498   rat. *J. Neurosci.* **13,** 2136–48 (1993).

499   39.   Lewin, G. R., Rueff, A. & Mendell, L. M. Peripheral and central mechanisms of NGF-
500   induced hyperalgesia. *Eur. J. Neurosci.* **6,** 1903–12 (1994).

501   40.   Korndörfer, I. P. & Skerra, A. Improved affinity of engineered streptavidin for the
502   Strep-tag II peptide is due to a fixed open conformation of the lid-like loop at the
503   binding site. *Protein Sci.* **11,** 883–93 (2002).

504   41.   Lapatsina, L. *et al.* Regulation of ASIC channels by a stomatin/STOML3 complex
505   located in a mobile vesicle pool in sensory neurons. *Open Biol.* **2,** 120096 (2012).

506   42.   van Hecke, O., Austin, S. K., Khan, R. A., Smith, B. H. & Torrance, N. Neuropathic
507   pain in the general population: a systematic review of epidemiological studies. *Pain*
508   **155,** 654–662 (2014).

509   43.   Bierhaus, A. *et al.* Methylglyoxal modification of Nav1.8 facilitates nociceptive
510   neuron firing and causes hyperalgesia in diabetic neuropathy. *Nat. Med.* **18,** 926–933
511   (2012).

512   44.   Abraira, V. E. & Ginty, D. D. The sensory neurons of touch. *Neuron* **79,** 618–639
513   (2013).

514   45.   Lechner, S. G. & Lewin, G. R. Hairy sensation. *Physiology (Bethesda).* **28,** 142–150
515   (2013).

516   46.   Syeda, R. *et al.* Chemical activation of the mechanotransduction channel Piezo1. *Elife*
517   **4,** (2015).

518   47.   Li, J. *et al.* Piezo1 integration of vascular architecture with physiological force. *Nature*
519   (2014). doi:10.1038/nature13701

520   48.   Ranade, S. S. *et al.* Piezo1, a mechanically activated ion channel, is required for
521   vascular development in mice. *Proc. Natl. Acad. Sci. U. S. A.* **111,** 10347–10352
522   (2014).

523   49.   Woo, S.-H. *et al.* Piezo2 is the principal mechanotransduction channel for

524   proprioception. *Nat. Neurosci.* **18,** 1756–62 (2015).

525   50.   Usoskin, D. *et al.* Unbiased classification of sensory neuron types by large-scale

526   single-cell RNA sequencing. *Nat. Neurosci.* **18,** 145–153 (2015).

527

528

Figure Legends

Figure 1 Screening for small molecules that modulate STOML3 oligomerization. **a**, Schematic representation of BiFC analysis of protein-protein interactions used for small molecule screen. **b**, Signal development observed when STOML3-VC was used as prey and VN-tagged STOML3 variants that do not properly oligomerize were used as bait. **c,** The normalized slope of BiFC signal development was used as a measure of oligomerization. ** $p < 0.01$ *** $p < 0.001$; unpaired t-test, two-tailed with $p = 0.0046$ (t=3.629 df=10) STOML3 *vs.* STOML3-V190P, $p < 0.0001$ (t=9.265 df=10) STOML3 *vs.* STOML3LR89,90VP, $p < 0.0001$ (t=12.15 df=10) STOML3 *vs.* un-transfected cells; numbers indicate replicate TECAN experiments derived from 4-6 independent transfections; data are shown as individual slopes and mean ± s.e.m. **d**, Structures of hit compounds, the oligomerization blockers, OB-1 and OB-2. **e,f**, Normalized slope of BiFC signal development in cells overexpressing Mus musculus or Homo sapiens STOML3 in the presence of OB-1 and OB-2 is shown. ** $p < 0.01$ *** $p < 0.001$; (i) unpaired t-test, two-tailed with p=0.0002 (t=6.594 df=8) mmSTOML3 *vs.* mmSTOML3 + OB-1, p=0.0064 (t=3.527 df=9) mmSTOML3 *vs.* mmSTOML3 + OB-2; numbers indicate replicate TECAN experiments derived from 4-6 independent transfections; data are displayed as individual slopes and mean ± s.e.m.; mean ± s.e.m. (e); (ii) Mann-Whitney *U* test, two tailed with p = 0.0002 (Sum of ranks 100 , 36 U 0) hsSTOML3 *vs.* hsSTOML3 + OB-1; numbers indicate replicate TECAN experiments derived from two independent transfections with 4 replicates each; data are shown as individual slopes and mean ± s.e.m. (f). **g**, Representative reconstructed *d*STORM images of STOML3-FLAG overexpressed in N2a cells. **h**, Distribution of STOML3-FLAG domain size as detected by *d*STORM imaging. ** $p < 0.01$ *** $p < 0.001$; unpaired t-test, two-tailed, with p = 0.0023 (t=3.496 df=20) STOML3 *vs.* STOML3-V190P, $p < 0.0001$ (t=6.533 df=26) STOML3 *vs.* STOML3 + OB-1, p = 0.0006 (t=3.994 df=23) STOML3 *vs.* STOML3 + OB-; numbers indicate N2a cells derived from at least 3 transfections. Each data point represents a single cell, for each cell the FHWM of 100 randomly chosen domains was measured.

Figure 2 Quantitative analysis of the effect of hit compounds on mechanotransduction. **a**, Schematic of pillar array analysis of mechanotransduction in N2a cells. **b**, Stimulus-response curves for N2a treated with either OB-1 or OB-2; both compounds significantly inhibit mechanically-gated currents in N2a cells. ** $p < 0.01$ *** $p < 0.001$; (i) Two-way ANOVA (stimulus response relationship) with p=0.0044 $F_{(1, 131)} = 8.390$ Vehicle *vs.* OB-

563   1, p = 0.0388 F (1, 108) = 4.375 Vehicle *vs.* OB-2, numbers indicate stimulus response

564   curves for N2a cells from > 5 independent experiments, data are displayed as mean of

565   individual bins ± s.e.m.; (ii) Mann- Whitney *U*-test, two-tailed, Bin 250-500 with p=0.0146

566   (U=27.00) Vehicle *vs.* OB1, p=0.0363 (U=23.50) Vehicle *vs.* OB2; numbers indicate cells

567   stimulated in this range, data are displayed as mean current amplitude of individual bins ±

568   s.e.m.. **c**, Hill plot of the concentration dependence of the OB-1 effect on the Piezo1 current

569   in N2a cells. ** p < 0.05; Mann-Whitney *U* test with p = 0.9266 Vehicle *vs.* 0.002µM OB-1,

570   p = 0.1236 Vehicle *vs.* 0.02µM OB-1, p = 0.1112 Vehicle *vs.* 2µM OB-1, p = 0.0105 Vehicle

571   *vs.* 20µM OB-1; numbers indicate N2a cells recorded in 2 (Vehicle), 4 (0.002µM), 3

572   (0.2µM), 3 (2µM), 3 (20µM OB1) independent experiments, data are displayed as mean

573   current amplitude of individual bins ± s.e.m.. **d**, Schematic of pillar array analysis of

574   mechanotransduction in acutely prepared DRG neurons. **e**, Stimulus-response curves for

575   mechanoreceptors treated with either OB-1 or OB-2; both compounds significantly inhibit

576   mechanically-gated currents activated by pillar deflections less than 50 nm, OB-1

577   significantly inhibits currents gated by deflections up to 250 nm. * p < 0.05 ** p < 0.01 ***

578   p < 0.001; (i) Two-way ANOVA with p = 0.0007 (F (1, 80) = 12.56) Vehicle *vs.* OB-1, p =

579   0.0017 (F (1, 78) = 10.59) Vehicle *vs.* OB-2; numbers indicate recorded stimulus-responses

580   curves of DRG mechanoreceptors from at least 3 DRG preps; (ii) unpaired t-test, two-tailed,

581   Bin 0-10 with p = 0.0462 (t=2.246 df=11) Vehicle *vs.* OB1, p = 0.0291 (t=2.477 df=12)

582   Vehicle *vs.* OB2; (iii) Mann-Whitney *U* test, two tailed, Bin 10-50 with p = 0.0053 Vehicle

583   *vs.* OB-1, p = 0.0068 Vehicle *vs.* OB-2, Bin 50-100 with p = 0.0224 Vehicle *vs.* OB-1, Bin

584   100-500 with p = 0.0239 Vehicle *vs.* OB-1; numbers indicate currents measured from DRG

585   mechanoreceptors, data from at least 3 DRG cultures derived from 5-7 weeks old mice; data

586   are displayed as current amplitude, each bin displayed as mean of cell averages ± s.e.m.. **f,**

587   Stimulus-response curves for nociceptors treated with either OB-1 significantly inhibit

588   mechanically-gated currents in these cells. * p < 0.05, (i) Two-way ANOVA with p =

589   0.0263 (F (1, 80) = 12.56) (F (1, 78) = 10.59) Vehicle *vs.* OB-1, *ns* (F (1, 78) = 10.59)

590   Vehicle *vs.* OB-2, numbers indicate stimulus-response curves in DRG nociceptors derived

591   from at least 3 DRG preparations derived from 5-7 weeks old mice ; data are displayed as

592   current amplitude, each bin displayed as mean of cell averages ± s.e.m; (ii) Mann-Whitney *U*

593   test with p =0.0388 (U=10.00, Bin 100-250) Vehicle *vs.* OB-1, p = 0.0087 (U=2.000, Bin

594   250-500) Vehicle *vs.* OB-2; numbers indicate currents measured in DRG nociceptors, at least

595   3 DRG preparations derived from 5-7 weeks old mice; data are displayed as current

596   amplitude, each bin displayed as mean of cell averages ± s.e.m.. **g-i,** In the presence of OB-1

597 there was no detectable difference in action potentials generated by current injection in either

598 (**h**) mechanoreceptors or (**i**) nociceptors, statistical tests applied: (i) Mann-Whitney *U* test

599 (Mechanoreceptors) with p = 0.215 (U=19); (ii) Student's t-test (Nociceptors), two-tailed

600 with p = 0.4743 (F=2.682, DFn=11, Dfd=12); numbers indicate cultivated neurons recorded

601 from 3 mice in 3 independent experiments; data are displayed as current amplitudes and mean

602 of individual bins ± s.e.m..

603

604 **Figure 3 Mechanoreceptors can be silenced with local OB-1 treatment.**

605 **a**, Inset: Electrical search protocol schema. A micro electrode (~1MΩ) was used to deliver

606 electrical stimuli at two distant points of the saphenous nerve trunk in order to trace

607 electrically identified units to their receptive fields. Proportions of mechano*IN*sensitive fibers

608 are shown. Three hours after local OB-1 treatment (250 -500 pmol OB-1 per paw) an increase

609 in mechanically *IN*sensitive Aβ-fibers was observed; note that mechanosensitivity had

610 recovered 24h post-injection. ** p < 0.01 *** p < 0.001; Fisher's exact test with p < 0.0001

611 Aβ-fibers Vehicle *vs.* OB-1(male & female mice), p < 0.0001 (Aβ-fibers Vehicle *vs.* OB-1

612 (male), p = 0.0033 Aβ-fibers Vehicle *vs.* OB-1(female), p = 1.0 (Aβ-fibers OB-1(male) *vs.*

613 OB-1 (female), p = 0.0028 Aβ-fibers OB-1 *vs.* OB-1 wash-out, p = 0.2465 Aδ-fibers Vehicle

614 *vs.* OB-1, p = 1.0 C-fibers Vehicle *vs.* OB-1; numbers indicate single sensory fiber recordings

615 derived from 10-20 independent experiments using adult mice (Fig 3a-e together), data are

616 displayed as percentage of individual fibers. **b,** Stimulus response function of C-MH fibers is

617 shown using a series of ascending displacements (32 – 1024 μm). C-MH fibers were

618 significantly less responsive in OB-1 treated mice compared to vehicle treated controls. * p <

619 0.05; Two-way ANOVA with p = 0.0412 (F=4.208, DFn=1, Dfd=257) Vehicle *vs.* OB-1;

620 numbers indicate fibers recorded in 10-20 independent experiments; data are displayed as

621 mean number of action potentials ± s.e.m.. **c,** Mean force thresholds for C-MH fiber

622 discharge are displayed showing a significant elevation of mechanical thresholds. * p < 0.05;

623 Mann-Whitney *U* test with p=0.0233 (U = 89); numbers indicate single sensory fiber

624 recordings derived from 10-20 independent experiments using adult mice (Fig 3a-e together);

625 data are displayed as individual thresholds and mean threshold ± s.e.m.. **d,** For C-M fibers

626 there was no significant difference between vehicle and OB-1 treated stimulus response

627 functions. Statistical test applied: Two-way ANOVA with p = 0.3563 (F=0,8579,DFn=1,

628 Dfd=115); numbers indicate single sensory fiber recordings derived from 10-20 independent

629 experiments using adult mice (Fig 3a-e together); data are displayed as mean number of

630 action potentials ± s.e.m.. **e**, Mean force thresholds for C-M fiber were also not different

631   between vehicle and OB-1 treatments. Statistical test applied: unpaired t-test, two tailed with

632   p = 0.7860 t=0,2756 df=18;numbers indicate single sensory fiber recordings derived from 10-

633   20 independent experiments using adult mice (Fig 3a-e together); data are displayed as

634   individual thresholds and mean threshold ± s.e.m.).

635

636   **Figure 4 OB-1 reduces the touch perception in mice**

637   A tactile perception task for head-restrained mice. **a,** Mice were trained to report a single

638   tactile pulse stimulus (inset shows stimulus voltage command pulse for all 8 amplitudes).

639   Trial structure: mice were trained to (1) hold the rest sensor and wait for a stimulus; (2) on

640   detection of the stimulus reach and press the target sensor within 500 ms from stimulus onset;

641   (3) obtain water reward by licking providing it was a successful trial. **b,** Psychometric curves

642   to different amplitude tactile stimuli are affected by injection of OB-1 into forepaw. Curves

643   were constructed with a sigmoid fitting of the mean hit rates to 7 different amplitudes of

644   tactile stimuli and a no stimulus trial (false alarm). Three conditions are displayed, injection

645   of the vehicle (black), injection of OB-1 (magenta) and a recovery session with no prior

646   injection (grey). **c,** OB-1 application to forepaw attenuates perception of near threshold tactile

647   stimuli. Grouped hit rates to 3 threshold amplitude values (125, 175 and 275 µm) from 5

648   mice were significantly reduced after OB-1 injection as compared to hit rates after vehicle

649   injection or on recovery session without prior injection. Statistical tests were made on hit

650   rates after subtraction of the corresponding false alarm rates. * $p < 0.05$; Wilcoxon Signed

651   Rank Test with p = 0.026 Vehicle *vs.*. OB-1, p = 0.0043 OB-1 *vs.*. OB-1 Wash-out, p = 0.12

652   Vehicle *vs.*. OB-1 Wash-out; numbers indicate mice treated, data are displayed as average of

653   individual hit rates of each mouse, grouped for 3 amplitudes ± s.e.m..

654

655   **Figure 5 Tactile-evoked pain can be treated with OB-1.**

656   **a,** Development of tactile-evoked pain after traumatic nerve injury is shown. Paw withdrawal

657   thresholds (PWT) to varying forces of von Frey filaments before and after unilateral CCI

658   were measured. Note that after nerve injury $Stoml3^{-/-}$ mice develop significantly less tactile-

659   evoked pain compared to wild type animals. *** $p < 0.001$ ** $p < 0.01$; Two-way ANOVA

660   with $p < 0.0001$ (F=107,65, DFn=1, Dfd=159) WT *vs. Stoml3$^{-/-}$* and Bonferroni's multiple

661   comparison with p > 0,9999, t = 1,488 df=159 (d0), p = 0,3728, t = 2,056 df = 159 (d2), p

662   = 0.0027, t = 3,701 df = 159 (d4), p = 0.0006, t = 4,104 df = 159   (d6), p = 0.006, t = 4,096

663   df = 159   (d8), p = 0.003, t = 4,273 df = 159   (d10), p < 0.0001, t =5,255df = 159   (d12), p

664   = 0.0303, t = 2,977 df = 159   (d14), p = 0.0048, t = 3,535 df = 159   (d21); numbers indicate

665 numbers of adult mice examined from two cohorts tested independently; data are displayed as

666 mean of individual median PWTs ± s.e.m.. **b,** Paw withdrawal latencies (PWLs) to a standard

667 radiant heat source applied to the ipsilateral hind paw of wild type and *Stoml3*^{-/-} mice before

668 and after CCI were not different between the genotypes. ** p < 0.01 * p < 0.05; Mann-

669 Whitney *U* test with p = 0.0065 WT (U = 1.500) naive *vs.* WT CCI, p = 0.0325 (U = 4.500)

670 *Stoml3*^{-/-} naive *vs. Stoml3*^{-/-} CCI, p = 0.2532 (U= 10.50) WT CCI *vs.* Stoml3^{-/-} CCI ; numbers

671 indicate mice treated (one cohort); data are displayed as mean PWL ± s.e.m.). **c**, Treatment of

672 naïve mice with OB-1 does not alter PWTs, paws of mice treated, (12= ipsi and contra;

673 6=ipsi, 6=contra) one cohort, *ns* Mann-Whitney *U* test with p = 0.2042 (U = 22) Naïve *vs*

674 OB-1 treated, p = 0.4545 (U = 14) OB-1 treated *vs.* Vehicle treated; numbers indicate adult

675 mice treated; data are displayed as mean of individual median PWTs. **d-e**, PWT measured

676 before and after nerve injury shows clear hypersensitivity that is not reversed by injection of

677 vehicle, note that local ipsilateral treatment of the neuropathic paw with OB-1 effectively

678 normalizes PWT, but treatment of the contralateral paw does not (e). ** p < 0.01 * p < 0.05;

679 (i) paired t-test, two tailed with p = 0.0028 (t=3,570 df=15) CCI male & female *vs.* CCI +

680 OB-1 male & female), p = 0.0066 (t=3,811 df=7) CCI male *vs.* CCI + OB-1 male, p = 0.0193

681 (t=3,022 df=7) CCI female *vs.* CCI + OB-1 female), (ii) Mann-Whitney *U* test with p= 0.25

682 (U = 7) CCI ipsi *vs.* OB-1contralateral injected ipsilateral measured; numbers indicate adult

683 mice examined from three cohorts tested independently; data are displayed as mean of

684 individual median PWTs; ± s.e.m.. **f,** Note that alleviation of hypersensitivity with OB-1

685 treatment is indistinguishable from gabapentin treatment. ** p < 0.01; Wilcoxon matched-

686 pairs signed rank test with p = 0.0013 (t=6,518 df=5) CCI *vs.* CCI + Gabapentin; numbers

687 indicate adult mice treated (one cohort tested), data are displayed as mean of individual

688 median PWTs; error bars indicate s.e.m.. **g,** Dose-response relationship of OB-1 is shown,

689 ED$_{50}$ = 4.42 µM or approximately 20 pmol. *** p < 0.001 ** p < 0.01; Mann-Whitney *U* test

690 with p = 0.7265 Vehicle *vs.* 0.5µM OB-1, p = 0.0749 Vehicle *vs.* 5µM OB-1, p = 0.0002

691 Vehicle *vs.* 50µM OB-1, p = 0.0044 Vehicle *vs.* 100µM OB-1; numbers indicate drug

692 treatments, adult mice came from 9 cohorts; data are displayed as mean of individual median

693 PWTs; error bars indicate s.e.m.. **h,** Measurement of PWTs over time; the maximal analgesic

694 efficacy developed between 3h and 9h after local OB-1 injection; numbers indicate mice

695 treated (one cohort tested); data are displayed as mean of individual median PWTs. **i,** No

696 significant change in PWT was measured in *Stoml3*^{-/-} mice with CCI after local

697 administration of OB-1, paired t-test with p =0.125 (Sum of signed ranks = 13.00 Number

698 of pairs = 6) CCI, *Stoml3*^{-/-} *vs.* CCI, *Stoml3*^{-/-} + OB-1; numbers indicate drug treatments (one

699 cohort tested); data are displayed as mean of individual median PWTs; error bars indicate

700 s.e.m.. **j,** S*toml3* copy number derived from lumbar DRG L4-6 determined using real-time

701 PCR showing an ipsilateral up-regulation of *Stoml3* mRNA. Note that the last two bars

702 represent data from *Stoml3*$^{-/-}$ mice. ** $p < 0.01$, * $p < 0.05$; Mann-Whitney *U* test with

703 $p=0.0079$ (U = 0) CCI ipsi *vs*. contra, $p=0.0357$ (U = 0) naive ipsi *vs*. CCI ipsi, $p=0.7000$ (U

704 = 4) naive ipsi *vs*. contra numbers indicate RNA preparations with L4-6 of two adult mice

705 pooled for one RNA preparation; data represent the mean copy number ± s.e.m.).

706

707 **Figure 6 Regulation of STOML3 in painful neuropathy**

708 **a,** Cytochemistry of lumbar DRGs from *Stoml3*$^{+/lacZ}$ mice that had received a nerve injury

709 (CCI). **b,** Note that the number of lacZ-positive neurons increased after a unilateral CCI

710 predominantly in large cells.***$p < 0.001$; Fisher's exact test with $p < 0.0001$; numbers

711 indicate cells counted analyzing 23 images obtained from 10 adult *Stoml3*$^{lacZ/lacZ}$ mice or 17

712 images obtained from adult *Stoml3*$^{+/lacZ}$ mice. **c**, schematic of the modified locus of StrepII

713 knockin mice. **d**, Western blots of protein extracts taken from the sciatic nerve of 2 adult

714 *Stoml3*$^{StrepII/StrepII}$ knockin mice per protein preparation subjected to unilateral CCI. Extracts

715 were made from two mice per time point note that a specific StrepII-STOML3 band was

716 detected ipsiliateral and contralateral to the injury at all time points (bands are not detected in

717 protein extracts from sciatic nerves of 2 adult *Stoml3*$^{-/-}$ mice per protein preparation). At day

718 2 (d2), day 6 (d6) and to a lesser extent day 13 (d13) post-injury there was clearly much more

719 protein found on the injured side compared to the uninjured sciatic nerve. The same protein

720 extracts were probed with antibodies against PGP9.5 a neuronal marker which decreased

721 dramatically on the injured side consistent with the known loss and atrophy of axons in the

722 CCI model.

723

724 **Figure 7 Inhibition of STOML3 alleviates painful diabetic neuropathy**

725 **a,** Diabetic peripheral neuropathy was induced using streptozotocin (STZ). After

726 development of peripheral neuropathy, diabetic mice received a single injection of OB-1 or

727 vehicle respectively into the plantar surface of the hind paw. **a,** Three hours after injection,

728 OB-1 treated mice showed attenuated mechanical sensitivity displayed as percentage of

729 withdrawal to increasing von Frey filaments. *** $p < 0.001$; Two-way ANOVA with $p >$

730 0.0001 ($F_{(1, 132)} = 28,07$) OB-1 *vs*. STZ and Bonferroni's multiple comparison with $p >$

731 0.9999 (t = 0,7867 df = 132) (0.07g), $p > 0.9999$ (t = 1.377 df= 132) (0.16g), $p = 0.0033$ (t =

732 3.539 df= 132) (0.4g), $p = 0.0123$ (t = 3.146 df= 132) (0.6g), $p = 0.0404$ (t = 2.753 df= 132)

733   (1g), p > 0,9999, t = 1.377 df= 132   (1.4g) ; numbers indicate adult mice treated; data are

734   displayed as mean of individual PWTs; error bars indicate s.e.m.) **b,** mechanical thresholds

735   required to elicit 60% withdrawal frequency.** $p < 0.01$, *** $p<0.001$; (i) Wilcoxon Signed

736   Rank Test with p = 0.0005 (Sum of signed ranks   -78,00   Number   of   pairs   12,   Naive   *vs.*

737   STZ, (ii) paired t-test, two-tailed with   p = 0.0013 (t=4,287 df=11) STZ *vs.* STZ + OB1, p =

738   0.0004 (t=4,939 df=11) STZ + OB1 *vs.* OB-1 Wash-out; numbers indicate mice treated, two

739   cohorts were   tested independently; data are displayed as mean of individual PWTs; error

740   bars indicate s.e.m.. **c,d**, Diabetic mice in the vehicle treated group showed no reversal of

741   mechanical hypersensitivity. ** $p < 0.01$ (i) ordinary Two-way ANOVA with p = 0.0765   (F

742   (1, 144) = 3,184) STZ vs. STZ+ Vehicle; (ii) Wilcoxon Signed Rank Test with p= 0.0765,

743   Naive *vs.* STZ; (ii) paired t-test, two-tailed with p= 0.3125 (t=1,054 df=1) STZ *vs.* STZ +

744   Vehicle, p=0.0859   (t=1,871 df=12) STZ + Vehicle *vs.* Vehicle Wash-out; numbers indicate

745   mice treated from two cohorts tested independently; data are displayed as mean of individual

746   PWTs; error bars indicate s.e.m.

747

Online Methods

The experiments in this study were carried out on adult inbred male or female mice (adult C57Bl/6n obtained from Charles River, Sulzfeld, Germany) or adult mice generated and breed in the laboratory (*Stoml3$^{-/-}$, Stoml3^{StrepII} or Stoml3^{lacZ}*). All experiments were performed in compliance with German and European laws for the use of animals in research and with appropriate permits from the Berlin authorities. Animals were kept under controlled temperature and a 12–h light, 12–h dark cycle with lights on at 06:00 A.M. Behavioral tests were conducted during the light phase. and the experimenter was blinded to treatment and genotype unless otherwise stated.

Statistics

All data were tested for normal distribution. Appropriate statistical tests applied for data analysis are referred to in the figure legend. Multiple comparisons were performed by repeated measures two-way ANOVA followed by Bonferroni post hoc test. Significance levels of $p < 0.05$ (*), $p < 0.01$ (**), and $p < 0.001$ (***) were used. Statistical analyses and exponential fits were made using the GraphPad Prism or Igor Pro 6.11. software. No statistical methods were used to pre-determine sample sizes but our sample sizes are similar to those reported in previous publications[1–11]. Experimenters were always blinded to treatment, or genotype unless otherwise stated. No special randomization procedures were used for assigning groups.

Molecular biology

Expression Constructs

Constructs for BiFC analysis were created by inserting the gene of interest, in frame, into the multiple cloning site of pBiFC-VC155 or pBiFC-VN173. Point mutations were introduced using PCR-based site-directed mutagenesis.

RT-PCR analysis

Lumbar L3-L6 dorsal root ganglia (DRG) were dissected from CCI and control mice, pooled and total RNA extracted with the TRIzol method (Invitrogen) as per manufacturer recommendations and treated with the TURBO DNA-free™ Kit to avoid DNA contamination. RNA was quantified using NanoDrop 2000 UV-Vis spectrophotometer (Thermo Scientific) and reverse-transcribed using SuperScript® III Reverse Transcriptase (Invitrogen). TaqMan Quantitative RT-PCR was used to detect the expression of STOML3 mRNA with 5´-GGAAGCCAGAGCCAAGGT-3´ and 5´-TGCAGGTACCGAAGTTGGA-3´primers in combination with the TaqMan probe #53 from Roche Universal Probe Library. Each sample was performed in triplicate in an ABI Prism 7700 Sequence Detection System (Thermo Scientific).

Cell culture

HEK-293 cells (passage numbers 4-20) were cultured in DMEM plus 10% fetal calf serum (FCS). Neuro2A (N2a) cells were cultured in DMEM/Opti-MEM media plus 10% FCS. Cell

lines were originally sourced from the ATCC and regularly checked for mycoplasma contamination. Sensory DRG neurons were isolated from 4 week old *Mus musculus* (C57Bl/6). Approximately 40 ganglia were collected from each mouse and individual cells were isolated by treating ganglia with 1 µg/ml collagenase IV for 30 min, followed by 1 ml of 0.05% trypsin, in PBS, for 5-20 min at 37°C. Enzyme-treated ganglia, in DMEM/F-12 media containing 10% Horse Serum (HS), were disrupted by gently passaging through a 20G needle; cells were then collected by centrifugation (1000 rpm, 3 min), washed and finally re-suspended in DMEM/F-12, 10% HS media (at no point were neurotrophins added to the culture). Experiments with isolated sensory neurons were conducted within 24-36 hours of isolation.

High through-put screen

HEK-293 cells were cultured to approximately 70% confluence; cells were co-transfected with plasmids encoding STOML3-VC and STOML3-VN using Fugene-HD, as per manufacturer's instructions. The transfection reaction proceeded for 8 h before cells were recovered and re-suspended in DMEM media containing 25 mM HEPES and lacking phenol red. Cells were plated on PLL-coated 384 well plates using an automated dispenser (EL406 Microplate Washer Dispenser). Plates already contained compounds from the ChemBioNet library (www.chembionet.info) a library containing small molecules with drug like properties[12]. Development of the YFP fluorescence signal was monitored overnight (15 h), with readings taken every 3 h (ex: 515 ± 8 nm, em: 535 ± 8 nm). Overnight monitoring of signal development was performed with a Freedom Evo workstation and a SafireII plate reader for fluorescence measurement (Tecan Group Ltd, Männedorf, Switzerland), and an integrated STX44-ICSA automated plate incubator (Liconic AG, Mauren, Liechtenstein). Experiments were repeated with 20 plates each day until the entire compound library had been screened and data was normalized to in-plate controls.

Compounds of interest were selected from the slope of YFP-signal vs time. Each well was compared to the average slope of in-plate positive controls (normalized percent activity), and compared to the mean and standard deviation of all samples on a plate (without the controls), giving a Z score as a measure of statistical significance[9]. One hundred and fifteen (115) inhibitors that significantly decreased the slope with a Z score < -3 were selected for further analysis. After re-screening in triplicate just 21 of the initially identified hit molecules were confirmed. Compounds that were themselves fluorescent or those that had significant effects on cell viability were discarded.

dSTORM imaging

N2a cells were cultured on EHS-Laminin coated precision coverglass, thickness 0.17mm, and transfected with a STOML3-FLAG plasmid. After overnight incubation, cells were treated for 3 hours with 20 µM compound, or DMSO as a control. Cells were fixed (15 min, 4% PFA), permeabilized (0.05% TritonX 100, 5 min) and blocked (phosphate buffered saline (PBS) containing 10% fetal goat serum (FGS), 37°C, 1 hr). Cells were labeled with mouse

831   anti-FLAG antibody (M2 clone Sigma #F1084, 1:100 in PBS containing 10% FGS). The
832   secondary antibody was an Alexa647-conjugated, goat anti-mouse antibody (1:100 in PBS
833   plus 10% FGS, 1 h, 37°C). After staining, the samples were fixed again. Prior to *d*STORM
834   imaging, coverslips were mounted in *d*STORM buffer PBS, pH 7.4, containing an oxygen
835   scavenger (0.5 mg/ml glucose oxidase), 40 mg/ml catalase, 10% (w/v) glucose and 100 mM
836   MEA [13].

837   The custom-built *d*STORM system, based on a Nikon Ti microscope, was described in detail
838   previously [14]. Before acquisition, we illuminated the Alexa647-labeled sample with 643 nm
839   to switch fluorophores into the OFF state. After molecules started blinking, we acquired a
840   sequence of frames (typically 10,000–20,000) using a 100x 1.49 NA objective, a 1.5
841   magnification lens and non-binned EMCCD array. An exposure time of 30 ms was used to
842   ensure good signal-to-noise and a high number of blinking single molecules/frame.

843   In order to aid drift correction PLL-coated Tetra-speck fluorescent beads were allowed to
844   adhere to the sample overnight. Localization: Single molecules were localized using open
845   source software rapidSTORM 3.2 [15]. The source images are first smoothed via median
846   operator followed by a fill-hole operation to reduce noise. In these 'de-noised' images,
847   rapidSTORM performs a Gaussian fit (Levenberg–Marquardt parameter estimation) to each
848   intensity spot, and fit quality and peak maxima were used as quality measures for
849   localization. This fit yields the precise position of the single molecule with sub-pixel
850   accuracy, the total intensity of the single molecule event and the frame number of the event.
851   Sample drift was corrected using fiduciary beads in the sample as reference points (custom
852   written algorithm, GREGOR).

853   For analysis of STOML3 domain size, all reconstructed images were blinded and then from
854   each imaged cell 100 individual dots were cropped (size: 20 x 20 pixels). A 2D-Gaussian fit
855   was calculated using the Igor software (WaveMetrics, USA). The x-width and y-width for
856   each dot were included in the data set as domains were not necessarily circular.

857

858   ***Chemical Synthesis***

859

860   The molecules OB-1 and OB-2 were structurally compared using a Tanimoto coefficient. The
861   structures were translated with a FCFP-4 protocol and the resulting fingerprints did not show
862   any significant similarity. Detailed chemical information for OB-1 and OB-2 can be found
863   with the following links:
864   OB-1 http://www.chemspider.com/Chemical-Structure.948385.html
865   OB-2 http://www.chemspider.com/Chemical-Structure.9820833.html
866   For de novo synthesis 5.6 g of ethyl-3-oxo-3-phenylpropanoate (29.06 mmol) was solubilized
867   in 50 ml toluene and 525 mg (1.45 mmol) of Cu(OTf)2 was added. Next, 1.57 g (14.5 mmol)
868   of benzoquinone was solubilized in 20 ml of toluene and added dropwise to the reaction
869   mixture followed by reflux for 3 h. The mixture was quenched with NH_4Cl and extracted
870   three times with ethyl acetate. The combined organic layers were washed with brine and
871   dried with Na_2SO_4. The crude product was purified by chromatography on silica gel eluting
872   with a gradient of Hex/EE (10:1) to give 2.24 g of ethyl-5-hydroxy-2-phenylbenzofuran-3-
873   carboxylate (Yield: 27 %) This product was an intermediate before final synthesis of OB-1.
874   Next 0.5 g (1.77 mmol) of ethyl-5-hydroxy-2-phenylbenzofuran-3-carboxylate was

875 solubilized in 20 ml DMF and 1.2 eq Cs2CO3 (0.7 g, 2.1 mmol), 0.1 eq CuI (33 mg, 0.17
876 mmol) and 285 mg (1.77 mol) 5-chloro-1-mehtyl-4-nitro-1H-imidazole were added. The
877 mixture was stirred for 3 h at room temperature. The organic solvent was removed under
878 reduced pressure. The crude product was purified by chromatography on silica gel eluting
879 with a gradient of Hex/EE (3:2) to give 644 mg of ethyl-5-(1-methyl-4-nitro-1H-imidazol-5-
880 yloxy)-2-phenylbenzofuran-3-carboxylate (Yield: 89 %).

881

882 *Electrophysiology*

883 Whole-cell, patch-clamp recordings were conducted as previously described[2,10], using patch
884 pipettes with a tip resistance of 3-6 MΩ, filled with a solution of: 110 mM KCl, 10 mM
885 NaCl, 1mM MgCl2, 1 mM EGTA and 10 mM HEPES, adjusted to pH 7.3 with KOH. For
886 experiments on DRG neurons 10 mM QX-314 was added to the pipette to block voltage-
887 gated sodium channels[10]. Extracellular solutions contained 140 mM NaCl, 4 mM KCl, 2 mM
888 $CaCl_2$, 1 mM $MgCl_2$, 4 mM glucose, 10 mM HEPES, adjusted to pH 7.4 with NaOH. A Zeiss
889 200 inverted microscope and an EPC-10 amplifier in combination with Patchmaster software
890 was used, data was analyzed using Fitmaster software (HEKA Electronik GmbH, Germany).
891 Mechanical stimuli were applied using a polished glass probe driven by the MM3A
892 micromanipulator (Kleindiek Nanotechnik, Germany). Mechanical stimuli were applied by
893 either; indenting the cell soma or by culturing cells on elastomeric pillar arrays and applying
894 the stimulus to the cell-substrate interface by deflecting an individual pilus. For a detailed
895 description of experiments using pillar arrays[10]. Images were obtained of the pilus before and
896 after deflection and images were analyzed off-line to determine the exact deflection for each
897 data point. Images were obtained using a 40x LD objective and a CoolSNAP EZ CCD
898 camera. The collection of stimulus-response data using pillar arrays generates data sets with
899 variation in both x and y. In order to effectively compare groups for each cell studied we
900 binned response data by stimulus size in the following bins: 0-10, 10-50, 50-100, 100-250,
901 250-500, 500-1000 nm. For each cell, current amplitudes within each bin were averaged and
902 then bins averaged between cells- we then tested for significance by testing whether the
903 current amplitude for a given stimulation range (i.e. bin) differed between samples. To
904 distinguish mechanoreceptors from nociceptors in the mixed population of acutely prepared
905 DRG neurons, the shape of the generated action potential (AP) was used. For quantitative
906 analysis of mechanosensitivity we measured responses in the most sensitive sub-population
907 of mechanoreceptors with APs lacking a hump in the falling phase and a full width at half
908 maximum (FWHM) of at least 0.7 ms, (average, ± s.e.m.: 0.9 ± 0.04 ms) [10].
909 To test the effect of compounds on stomatin modulation of ASIC currents CHO cells were
910 transfected with vectors encoding Stomatin and ASIC3, in a ratio of 4:1 using lipofectamine,
911 as per manufacturer's instructions. Cells were incubated with 20 µM OB-1 for 3 hours in
912 extracellular buffer (see above), and OB-1 was maintained in the media during
913 electrophysiological experiments. ASIC3 channels were gated by applying solutions of pH6
914 and pH4, and both the transient and sustained peak current density was measured.

915

916 *Ex vivo skin nerve preparation*

917 The skin-nerve preparation was used essentially as previously described to record from single
918 primary afferents[7]. For the electrical search protocol a microelectrode (1MΩ) was
919 maneuvered to contact the epineurium of the nerve trunk and an electrical stimulation was
920 delivered at 1 s intervals with square wave pulses of 50 – 500 ms duration. In most filaments
921 3-5 single units were counted. The electrical nerve stimulation was done at 2 distant sites of
922 the saphenous nerve to trace electrically identified units to their receptive fields. Mechanical
923 sensitivity of single units was tested by mechanical stimulation with a glass rod. A computer-
924 controlled nanomotor (Kleindiek, Reutlingen, Germany) was used to apply controlled
925 displacement stimuli of known amplitude and velocity. The probe was a stainless steel metal
926 rod and the diameter of the flat circular contact area was 0.8 mm containing a force
927 transducer (Kleindiek, Reutlingen, Germany). The signal driving the movement of the linear
928 motor and raw electrophysiological data were collected with a Powerlab 4.0 system
929 (ADInstruments) and spikes were discriminated off-line with the spike histogram extension
930 of the software.
931
932 **_Tactile perception task_**
933
934 Male C57Bl6/J mice were anaesthetized and a lightweight metal headholder was implanted to
935 the skull using glue (Loctite 401, Henkel) and dental cement (Paladur®, Heraeus). Mice were
936 habituated to the head-restraint and the behavioral setup over 1-2 days. Mouse licking and
937 forepaw behavior was monitored with three custom-made capacitance sensors: a licking
938 sensor, a rest sensor and a target sensor that provided an online monitor of paw or tongue
939 contact. The rest sensor was a ball (diameter: 6 mm) mounted on a glass rod of 30 mm length,
940 glued to a piezoelectric bender (PICMA® Multilayer Piezo Bender Actuator, Physik
941 Instrumente). The piezo generated a 30 ms cosine tactile pulse via a piezo amplifier system
942 (Sigmann Elektronik). The stimulus amplitude was calibrated with a high-speed (300 Hz)
943 camera (Dalsa Genie HM640). The target sensor (diameter: 6 mm) had a start position of 10
944 mm horizontally in front of the rest sensor and was attached to a Fisso 3D articulated arm on
945 a linear translation stage (ST9-100-2 eco-P, ITK Dr. Kassen GmbH, Germany). Mice were
946 water restricted and given approximately 4 x 0.6 µl water rewards on condition of touching
947 the target sensor within a defined latency from stimulus onset and licking the water dispenser.
948 The target sensor moved to the start position at the start of a new trial and away from the
949 mouse at the end of the trial. Inter-trial interval was randomized between 7 and 13 s. White
950 noise was played throughout the trial. The response window (rewarded stimulus-to-touch
951 latency) was reduced during behavioral training to 500 ms during the testing session. Mice
952 were trained with high amplitude stimuli (620 µm) and then tested in the same session with
953 seven different stimulus amplitudes (in µm: 45, 80, 125, 170, 275, 385, 620) and a no-
954 stimulus trial to calculate the false alarm rate. Stimuli were presented in a randomized order.
955 The setup was controlled with custom written software in LabView 10.0 (National
956 Instruments 2010). Drug injections of OB-1 or DMSO alone were dissolved in Ringer's
957 solution (in mM: 135 NaCl, 5 KCl, 5 HEPES, 1.8 CaCl2, 1 MgCl2) to make the OB-1 and
958 vehicle solution. Approximately 5 µl was injected into the digits with a glass micropipette
959 and 10 µl into the palm with a Hamilton syringe. During the injection procedure, the mouse

960 was anaesthetized with isoflurane (1.5 to 2.0 % in O2). The experimenter was not blinded to
961 treatment.
962 To construct the psychometric curves we first averaged the rates of pressing the target sensor
963 within 500 ms from stimulus onset across 5 mice. Next we fitted the data with a sigmoid
964 function in Igor Pro 6.11 (WaveMetrics):

965 $$f(x) = base + \frac{max}{1+\exp(\frac{xY50-x}{slope})}$$

966 *Mouse Pain Models and Behavioral Experiments*

967 *Chronic Constriction Injury*
968 In deeply anaesthetized mice using isoflurane delivered in 100% O_2 (Univentor 410
969 Anaesthesia unit; Univentor, Malta), four loose silk (5/0; Catgut GmbH Markneukirchen)
970 ligatures were placed around the sciatic nerve at the level of the right mid-thigh as described
971 previously[5].
972

973 *Spared Nerve Injury*
974 In deeply anesthetized mice (see above) a skin and muscle incision was made at the thigh to
975 reveal the sciatic trifurcation. Distal to the sciatic's trifurcation, nerve pieces (2-4 mm) of the
976 sural as well as the common peroneal nerves were removed leaving the tibial nerve intact. In
977 sham controls the surgery was performed without transecting the nerves. Wounds were
978 closed with wound clips before anesthesia was terminated.
979

980 *NGF-induced Hyperalgesia*
981

982 A single dose of NGF (1 μg/g body weight) was injected intraperitoneal (i.p.) into adult mice
983 and behavioral testing was performed 6h, 24h, 48h, and 72 hours post injection.

984 *Diabetic Neuropathy Model*
985 Eight week old C57Bl/6 mice were used for diabetes experiments. Diabetes was induced
986 using previously reported protocols [11,16]. Briefly, 6 consecutive intraperitoneal injections of
987 streptozotocin (STZ, Sigma-Aldrich, # S0130) were given with 24h intervals at 60 mg/Kg
988 body weight in citrate buffer (0.05 M, pH 4.5) to induce diabetes. Blood glucose was
989 maintained between 400 and 500 mg/dL throughout the experimental period. Mechanical
990 sensitivity was measured and only those mice showing increased sensitivity to von Frey
991 filaments as compared to basal sensitivity were selected for OB-1 testing. Vehicle or OB-1
992 (approximately 20 μl solution, 250 pmol per paw) was injected subcutaneously into
993 intraplantar surface of diabetic mice under mild isoflurane anesthesia and mechanical
994 sensitivity was measured from both injected (ipsilateral) and non-injected (contralateral)
995 paws at 4 and 24h post-injection.
996

997 *Assessing pain behavior.*
998 Mice were allowed to habituate to the testing apparatus (acrylic chambers 10 × 10 cm in size,
999 suspended above a wired mesh grid) one hour prior to behavioral testing. Calibrated von-Frey

1000 hair monofilaments (Aesthesio® set of 20 monofilaments, Ugo Basil) were applied to the
1001 plantar surface of the hind paw in order to deliver target forces from 0.008 grams to 4 grams
1002 increasing in an approximately logarithmic scale. A single von Frey stimulus lasted for two
1003 seconds unless the mouse withdrew its paw. The up-and-down method described by Chaplan
1004 [8] was adapted as follows: Testing began with a 0.4 g filament applied three times A positive
1005 response was noted if paw withdrawal was seen to all three stimuli, so that the next smallest
1006 filament was tested next. A negative response was noted when paw withdrawal was not seen
1007 to at least one stimulus which was followed by testing with the next largest filament. Paw
1008 withdrawal thresholds were calculated as the median of 23 to 30 determined turning points.
1009
1010 A focused, radiant heat light source (IITC Life Science Inc.) was used to measure paw
1011 withdrawal thresholds to heat as previously described. The light beam created a focused spot
1012 of 4x6 mm on the hind paw. The time to paw withdrawal in response to a constantly
1013 increasing heat stimulus (maximal active intensity = 25% of the light source) with a cutoff of
1014 20 seconds was determined. Heat stimuli were repeated 6 times for each paw with a stimulus
1015 interval of 1 minute.
1016

1017 *Generation of Stoml3^{LacZ} and Stoml3^{StrepII} mice*

1018 The C57BL/6J mouse BAC clones (https:bacpac.chori.org) containing the *Stoml3* gene was
1019 isolated from RPCI-23 library[17]. A 12-kb DNA fragment containing the exon1 and its
1020 flanking regions of *Stoml3* gene was isolated by gap repair[18]. Homologous recombination in
1021 bacteria [18,19] was used to fuse an NLS-lacZ cassette to the ATG of *Stoml3* and to introduce
1022 the self-excision neo cassette [20] into the *Stoml3* locus. Similarly, homologous recombination
1023 in bacteria was used to introduce a Strep-TagII after the ATG of *Stoml3* and a neomycin
1024 cassette flanked by two loxP into the first intron of *Stoml3* locus to generate the *Stoml3^{StrepII}*
1025 allele. In both targeting vectors the MC1-diphteria toxin A (DTA) cassette was placed at the
1026 3' end of the vector and was used for negative selection. Colonies of the E14.1 ES cell line
1027 (129/Ola) that had incorporated the targeting vector into their genome were selected by G418
1028 and analyzed for homologous recombination by Southern blot analysis using 5' and 3' probes
1029 that lie outside of the targeting vector. Two clones were microinjected into C57BL/6
1030 blastocysts to generate chimeras that transmitted the *Stoml3^{LacZ}* allele or the *Stoml3^{StrepII}*
1031 allele.
1032 The *Stoml3^{LacZ}* strain was genotyped using Stoml3-LacZ F: gac agt gtg atg tca ggg aag; LacZ
1033 int R: cct tcc tgt agc cag ctt tca tc, Stoml3-LacZ R: cct tgt aaa ctg ata gcg ggg ac primers. The
1034 *Stoml3^{StrepII}* strain was genotyped using Stoml3-Strep F: gta gca gtg ttg ttt aga aag together
1035 with Stoml3-StrepII R2 gct agc cat ggc tca ttc ttg for the mutant allele or with Stoml3-Strep
1036 R1 aca gtg atg atg tcc cag c for the wild type allele.
1037
1038 The *Stoml3^{StrepII}* allele could conceivably negatively alter the function of the STOML3
1039 protein. We thus generated homozygous *Stoml3$^{StrepII/StrepII}$* mice and used the ex vivo skin
1040 nerve preparation to determine if cutaneous mechanorecpetors lose mechanosensitivity in this
1041 strain. Recordings from 4 wild type littermate controls and 4 *Stoml3$^{StrepII/StrepII}$* mice revealed

no significant differences in the incidence of mechanoinsensitive fibers between the genotypes. Amongst Aβ-fibers mechanoinsensitive fiber incidence was 1/21 (5%) and 0/23 (0%) for wild type and $Stoml3^{StrepII/StrepII}$ mice respectively Amongst Aδ-fibers mechanoinsensitive fiber incidence was 0/12 (0%) and 1/11 (9%) for wild type and $Stoml3^{StrepII/StrepII}$ mice, respectively.

Histochemistry

Mice were perfused with ice-cold PBS followed by 0.5% gluteraldehyde for 20 minutes. Post-fixed lumbar DRGs were washed several times in PBS and cryoprotected in 30% sucrose overnight at 4°C. DRGs were embedded in O.C.T. Tissue-Tek (Sakura Finetek, Netherland) on dry ice and stored at -80°C. Tissue was on a Cryostat CM3050S (Leica) and slides were incubated in X-gal reaction buffer (35 mM potassium ferrocyanide, 35 mM potassium ferricyanide, 2mM MgCl2, 0.02% Nonidet P-40, 0.01% Na deoxycholate and 1 mg/ml of X-Gal) for 2 days at 37°. Slices were washed several times in PBS until the solution no longer turned yellow, air-dried and sealed with a coverslip.

Sections were observed on a Zeiss Axiovert 135 microscope using Zen imaging software (Zeiss, Germany). Image J (NIH, USA) was used to manually trace the outlines of cell in order to obtain cell area. Electron microscopy was performed on nerves using standard methods as previously described[7].

Western blotting

Tissues from $Stoml3^{StrepII/StrepII}$ and control mice were lysed with 8 M urea buffer and protein concentration was determined using the Bradford reagent. Proteins were separated by SDS-PAGE, followed by Western blot analysis using mouse Strep-tagII antibody (2-1507-001, IBA), PGP 9.5 antibody (ab10404, Abcam) and mouse anti β actin (A1978, Sigma). Appropriate horseradish peroxidase-conjugated secondary antibodies were used for chemiluminescence (ECL, Millipore or Supra, Thermo scientific SuperSignal).

Methods only references

1. Lechner, S. G. & Lewin, G. R. Peripheral sensitisation of nociceptors via G-protein-dependent potentiation of mechanotransduction currents. *J. Physiol.* **587,** 3493–3503 (2009).
2. Chiang, L.-Y. *et al.* Laminin-332 coordinates mechanotransduction and growth cone bifurcation in sensory neurons. *Nat. Neurosci.* **In Press,**
3. Hu, J. & Lewin, G. R. Mechanosensitive currents in the neurites of cultured mouse sensory neurones. *J. Physiol.* **577,** 815–828 (2006).
4. Brand, J. *et al.* A stomatin dimer modulates the activity of acid-sensing ion channels. *EMBO J.* **31,** 3635–3646 (2012).
5. Wetzel, C. *et al.* A stomatin-domain protein essential for touch sensation in the mouse. *Nature* **445,** 206–209 (2007).
6. Lechner, S. G., Frenzel, H., Wang, R. & Lewin, G. R. Developmental waves of mechanosensitivity acquisition in sensory neuron subtypes during embryonic

1086   development. *EMBO J.* **28,** 1479–1491 (2009).

1087   7.   Moshourab, R. A., Wetzel, C., Martinez-Salgado, C. & Lewin, G. Stomatin-domain
1088   protein interactions with acid sensing ion channels modulate nociceptor
1089   mechanosensitivity. *J. Physiol.* (2013). doi:10.1113/jphysiol.2013.261180

1090   8.   Chaplan, S. R., Bach, F. W., Pogrel, J. W., Chung, J. M. & Yaksh, T. L. Quantitative
1091   assessment of tactile allodynia in the rat paw. *J. Neurosci. Methods* **53,** 55–63 (1994).

1092   9.   Brideau, C., Gunter, B., Pikounis, B. & Liaw, A. Improved statistical methods for hit
1093   selection in high-throughput screening. *J. Biomol. Screen.* **8,** 634–647 (2003).

1094   10.   Poole, K., Herget, R., Lapatsina, L., Ngo, H.-D. & Lewin, G. R. Tuning Piezo ion
1095   channels to detect molecular-scale movements relevant for fine touch. *Nat. Commun.*
1096   **5,** 3520 (2014).

1097   11.   Bierhaus, A. *et al.* Methylglyoxal modification of Nav1.8 facilitates nociceptive
1098   neuron firing and causes hyperalgesia in diabetic neuropathy. *Nat. Med.* **18,** 926–933
1099   (2012).

1100   12.   von Kleist, L. *et al.* Role of the Clathrin Terminal Domain in Regulating Coated Pit
1101   Dynamics Revealed by Small Molecule Inhibition. *Cell* **146,** 471–484 (2011).

1102   13.   Heilemann, M. *et al.* Subdiffraction-resolution fluorescence imaging with conventional
1103   fluorescent probes. *Angew. Chem. Int. Ed. Engl.* **47,** 6172–6176 (2008).

1104   14.   Lampe, A., Haucke, V., Sigrist, S. J., Heilemann, M. & Schmoranzer, J. Multi-colour
1105   direct STORM with red emitting carbocyanines. *Biol. Cell* **104,** 229–237 (2012).

1106   15.   Wolter, S. *et al.* rapidSTORM: accurate, fast open-source software for localization
1107   microscopy. *Nat. Methods* **9,** 1040–1041 (2012).

1108   16.   Vareniuk, I., Pavlov, I. A. & Obrosova, I. G. Inducible nitric oxide synthase gene
1109   deficiency counteracts multiple manifestations of peripheral neuropathy in a
1110   streptozotocin-induced mouse model of diabetes. *Diabetologia* **51,** 2126–2133 (2008).

1111   17.   Osoegawa, K. *et al.* Bacterial artificial chromosome libraries for mouse sequencing
1112   and functional analysis. *Genome Res.* **10,** 116–128 (2000).

1113   18.   Lee, E. C. *et al.* A highly efficient Escherichia coli-based chromosome engineering
1114   system adapted for recombinogenic targeting and subcloning of BAC DNA. *Genomics*
1115   **73,** 56–65 (2001).

1116   19.   Liu, P., Jenkins, N. A. & Copeland, N. G. A highly efficient recombineering-based
1117   method for generating conditional knockout mutations. *Genome Res.* **13,** 476–484
1118   (2003).

1119   20.   Bunting, M., Bernstein, K. E., Greer, J. M., Capecchi, M. R. & Thomas, K. R.
1120   Targeting genes for self-excision in the germ line. *Genes Dev.* **13,** 1524–1528 (1999).
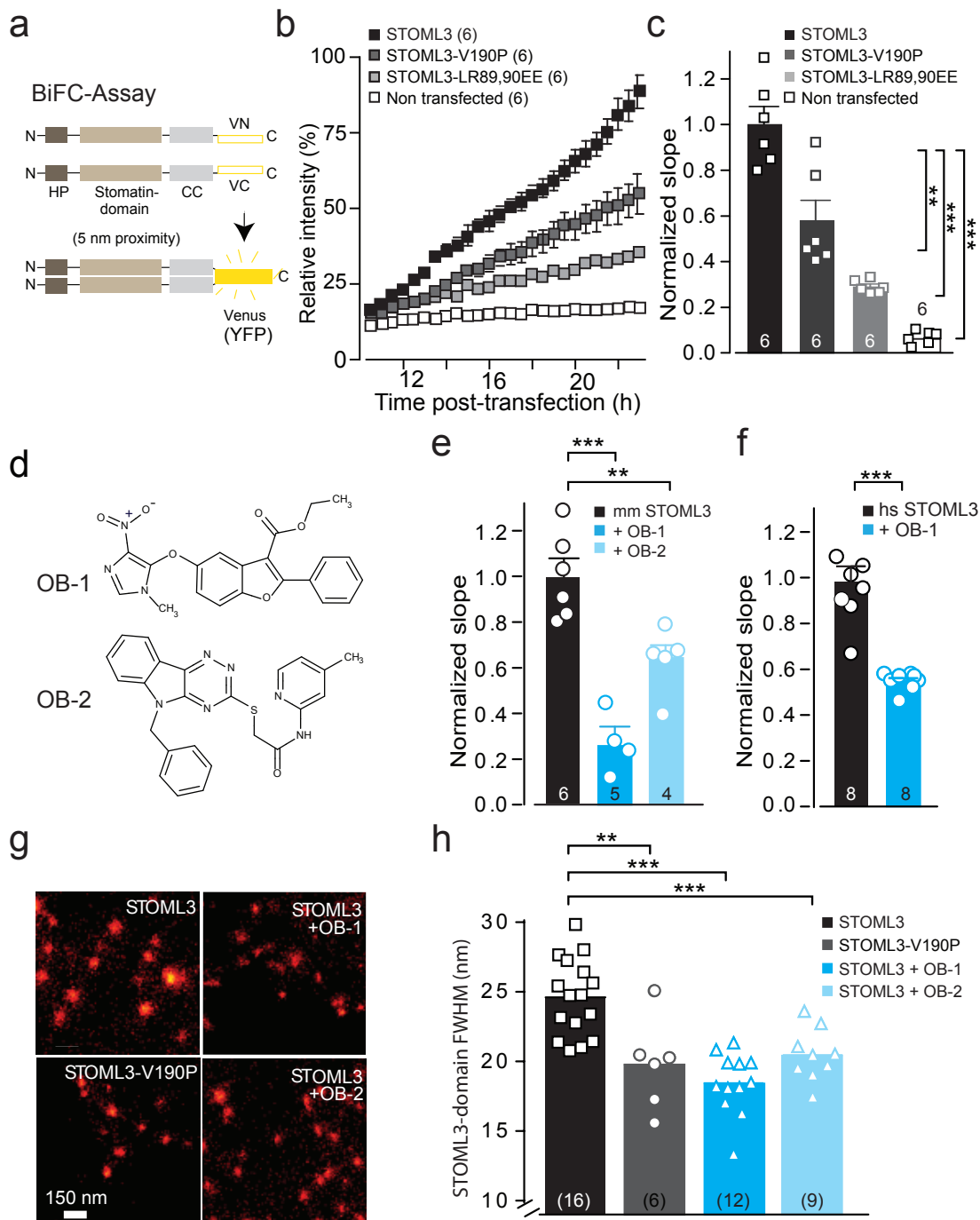
1121

1122

1123

1124

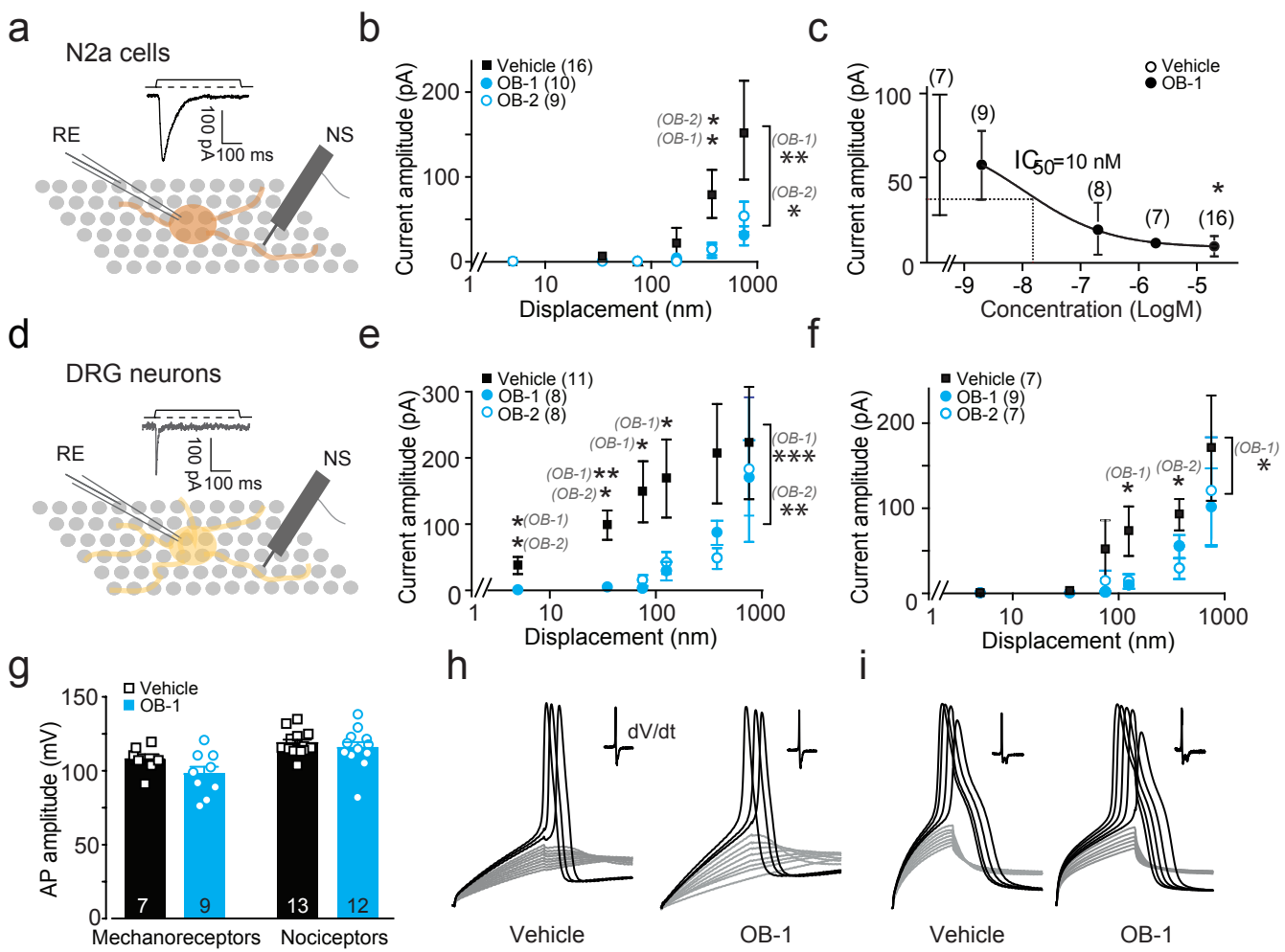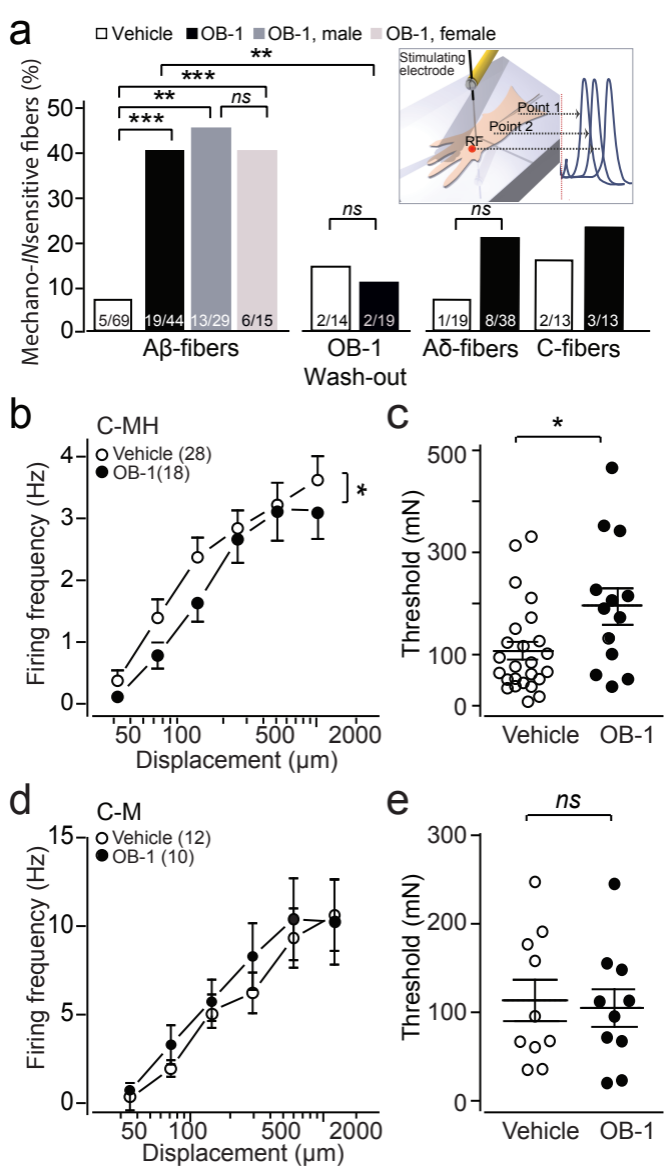# Figure 1

a N2a cells

RE   NS
100 pA
100 ms

b
Current amplitude (pA)
- Vehicle (16)
- OB-1 (10)
- OB-2 (9)

(OB-2) *
(OB-1) *
(OB-1) **
(OB-2) *

Displacement (nm)

c
Current amplitude (pA)
○ Vehicle
● OB-1

IC$_{50}$=10 nM

(7)
(9)
(8)
(7)
(16)
*

Concentration (LogM)

d DRG neurons

RE   NS
100 pA
100 ms

e
Current amplitude (pA)
- Vehicle (11)
- OB-1 (8)
- OB-2 (8)

(OB-1) *
(OB-2) *
(OB-1) **
(OB-2) *
(OB-1) *
(OB-1) *
(OB-1) ***
(OB-2) **

Displacement (nm)

f
Current amplitude (pA)
- Vehicle (7)
- OB-1 (9)
- OB-2 (7)

(OB-1) *
(OB-2) *
(OB-1) *

Displacement (nm)

g
AP amplitude (mV)
□ Vehicle
○ OB-1

7   9   13   12
Mechanoreceptors   Nociceptors

h
dV/dt

Vehicle   OB-1

i

Vehicle   OB-1

Figure 2

Figure 3

Figure 4

Figure 5

a

CCI, contralateral

Stoml3$^{+/lacZ}$, lacZ-positive cells
Stoml3$^{+/lacZ}$, lacZ-negative cells

Frequency (number)
Cell diameter (μm)

CCI, ipsilateral

30μm

Frequency (number)
Cell diameter (μm)

b

Proportion (%)

***

351   458

lacZ-negative

lacZ-positive

105   55

Ipsi   Contra

c

Stoml3^{StrepII} allele

0   StrepII E1   E2 E3   E4   E5   E6   E7   33572 nt

1 kb

STOML3^{StrepII} protein

MASWSHPQFEKGGGSGGGSGGGSWSHPQFEKGADSPEKLEKNNLV

StrepII   StrepII

d

CCI

d2   d6   d13   Stoml3StrepII   Stoml3 KO

c   i   c   i   c   i   kDa

STOML3
StrepII   —35

—25

PGP 9.5   —25

β-actin

Figure 6

Figure 7